의학박사 학위논문

Study of the effects of miR-200 overexpression and LOXL4 downregulation on triple-negative breast cancer progression

miR-200의 과발현과 LOXL4 발현 억제가 삼중음성 유방암 진행에 미치는 영향에 관한 연구

2017년 8월

서울대학교 대학원

의과학과

최 슬 기

A thesis of the Degree of Doctor of Philosophy

miR-200의 과발현과 LOXL4 발현 억제가 삼중음성유방암 진행에 미치는 영향에 관한 연구

Study of the effects of miR-200 overexpression and LOXL4 downregulation on triple-negative breast cancer progression

August 2017

The Department of Biomedical Sciences,

Seoul National University

College of Medicine

Sul Ki Choi

ABSTRACT

Study of the effects of miR-200 overexpression and LOXL4 downregulation on triple-negative breast cancer progression

Sul Ki Choi

Biomedical Sciences
The Graduate School
Seoul National University

Introduction: The microRNA-200 (miR-200) family is known to have a pivotal role in regulating epithelial to mesenchymal transition through the suppression of transcription factors of E-Cadherin, ZEB1, and ZEB2, but the role of miR-200 family in the migration and invasion of breast cancer cells is controversial. The lysyl oxidase-like 4 (LOXL4), a member of the lysyl oxidase (LOX) family, is involved in extracellular matrix (ECM) modulation and signaling pathway related to cancer cell growth and survival.

However, the role of LOXL4 in breast cancer progression and metastasis is still unclarified. This study investigated the mechanisms by which the miR-200 family modulated the migratory and invasive abilities of aggressive triple-negative breast cancer (TNBC) cells, which have the worst prognosis among breast cancer subtypes. In addition, the role of LOXL4 in tumor formation and metastasis in TNBC was investigated and overall survival (OS) was analyzed to evaluate its clinical significance as a prognostic factor in TNBC patients.

Methods: The miR-200 family (miR-200b/200a/429 and miR-141/200c clusters) coupled with green fluorescence protein (GFP), the LOXL4 shRNA (shLOXL4) coupled with red fluorescence protein (RFP) and the firefly luciferase (Luc) coupled with GFP were transduced into MDA-MB-231 cells, TNBC cells, using a lentiviral system. Gene expression was evaluated using real-time polymerase chain reaction (PCR) or reverse transcriptase-PCR (RT-PCR). The migratory and invasive abilities were assessed using trans-well or wound-healing assays. The secreted cytokines and growth factors from cells were quantified using a Bio-Plex 200 multiplex array system. Western blot and immunofluorescence

staining were conducted to investigate the signaling pathways. The xenograft tumor models were produced by injection with breast cancer cells into the mammary gland or tail vein of 6-week old female Balb/c nude mice for an orthotopic or lung metastatic model, respectively. Primary tumor volumes were measured by a digital caliper. The primary tumor in mammary gland and metastatic lung burden were obtained using IVIS and Maestro imaging system. Histological analysis was assessed by H&E, Picrosirius red, Masson's trichrome and immunostaining. Second harmonic generation (SHG) imaging was conducted to quantify the collagen fiber lengths, straightness, and widths. A public database (BreastMark) for overall survival (OS) was used to examine the prognostic value of the LOXL4, collagen I, and collagen IV genes in breast cancer patients.

Results: The overexpression of the miR-200b/200a/429 or miR-141/200c cluster suppressed cell growth, but significantly increased migration and invasion of MDA-MB-231 cells, and led to an increase in the phosphorylation of focal adhesion kinase (FAK) and protein kinase B (AKT). Chemical inhibitors of FAK and

phosphatidylinositol-4,5-bisphosphate 3-kinase (PI3K)/AKT suppressed the migration and invasion of MDA-MB-231 cells which was enhanced by the overexpression of the miR-200b/200a/429 or miR-141/200c cluster. Compared to the miR-200b/200a/429 cluster-transduced MDA-MB-231 cells, the miR-141/200c cluster-transduced MDA-MB-231 cells exhibited a significant increase in vascular endothelial growth factor (VEGF)-A secretion and integrin-alphaV (integrin-αV) expression. Treatment with an anti-VEGF-A-neutralizing antibody inhibited the increase in migration and invasion and significantly reduced the phosphorylation of FAK and AKT in the miR-200b/200a/429- or miR-141/200c-transduced MDA-MB-231 cells. In the mouse xenograft models, LOXL4 knockdown increased the primary tumor growth and lung colonization in MDA-MB-231 cells. LOXL4 knockdown caused a significant increase in the levels of collagen I and IV, as well as lysine hydroxylase (PLOD)1, PLOD2, prolyl 4-hydroxylase subunit alpha (P4HA)1, and P4HA2, which are the key enzymes in collagen biogenesis. The collagen bundle thickening was observed in LOXL4 knockdown tumors as compared with that of control tumors. The OS analysis of the breast cancer patients (n =

584) revealed that low LOXL4 expression and combination of low LOXL4 and high collagen I and IV expression were significantly correlated with a poor OS, particularly, TNBC patients (n = 101).

Conclusions: This study demonstrates the miR-141/200c cluster promotes the migratory and invasive abilities of MDA-MB-231 cells through FAK- and PI3K/AKT-mediated signaling by means of increased VEGF-A secretion. In addition, the low LOXL4 expression triggered the ECM remodeling by inducing the collagen synthesis, deposition, and structural changes, which resulted in a significant promotion of tumor growth and metastasis. LOXL4 might be used as a prognostic marker in TNBC patients.

Keywords: Triple-negative breast cancer (TNBC), microRNA-200 (miR-200), vascular endothelial growth factor (VEGF), Lysyl oxidase-like 4 (LOXL4), Collagen, Tumor progression, Overall survival

Student Number: 2012-31164

CONTENTS

LIST OF TABLES AND FIGURES

LIST OF ABBREVIATIONS

miR-200: microRNA-200

TNBC: triple-negative breast cancer

VEGF: vascular endothelial growth factor

PI3K: phosphatidylinositol-4,5-bisphosphate 3-kinase

AKT: protein kinase B

FAK: focal adhesion kinase

LOXL4: lysyl oxidase (LOX)-like 4

ECM: extracellular matrix

SHG: second harmonic generation

PLOD: lysine hydroxylase

P4HA: prolyl 4-hydroxylase subunit alpha

OS: overall survival

Chapter 1

Overexpression of the miR-141/200c cluster promotes the migratory and invasive ability of triple-negative breast cancer cells through the activation of the FAK and PI3K/AKT signaling pathways by secreting VEGF-A

INTRODUCTION

Aberrant expression of microRNAs (miRs), which are small non-coding RNA molecules consisting of approximately 22 nucleotides, has been identified in human cancer, where the miRNA signature is associated with specific clinic and biological features [1]. The microRNAs related to cancers may act as tumor suppressors or oncogenes, depending on the cancer type [2, 3]. The miR-200 family member genes are clustered at two locations in the genome: the miR-200b/200a/429 cluster and the miR-200c/141 cluster [4]. The miR-200 family members repress the epithelial-to-mesenchymal transition (EMT), cancer cell migration, tumor growth, and metastasis by directly targeting specific genes, such as ZEB1, Suz12, moesin, and AP-2γ [4, 5]. In contrast, the miR-200 family members have been shown to enhance the migration ability of breast cancer cells and to promote the metastatic colonization of breast cancer cells through up-regulating the expression of E-cadherin and down-regulating that of ZEB2 and Sec23a [6, 7]. In a recent study, high expression of the miR-200 family was associated with a high probability of relapse, poor survival, and distant metastasis in breast cancer patients [8]. The loss of miR-200c expression has also been related to the induction of an aggressive, invasive, and chemoresistant phenotype of non-small cell lung cancer

[9]. Conflicting results have been obtained in studies of the role of each miR-200 family member in repressing or enhancing cancer cell migration and invasion as well as the tumor growth and metastasis of diverse cancers, including breast cancer [10, 11].

Triple-negative breast cancer (TNBC), i.e., breast cancer lacking estrogen receptor (ER), progesterone receptor (PR), and human epidermal growth factor receptor 2 (HER2) expression, is a highly invasive and metastatic form of breast cancer with a generally poorer prognosis than that of other breast cancer subtypes [12]. It is important to develop new treatment strategies based on a better understanding of the underlying mechanisms regulating the aggressive behavior of TNBCs. TNBCs express the miR-200 family members at a significantly lower level than do other subtypes of breast cancer, such as ER-positive or HER2-positive breast cancer [13]. Only a small number of the miR-200 target genes that are involved in breast cancer cell migration and metastasis have been identified [4-6], and few studies of the role of the miR-200ab or miR-200c cluster in human TNBC have been conducted. The biological relevance of the function of the miR-200ab or miR-200c cluster in human TNBC remains to be discovered.

Synthetic miR-200b directly downregulates vascular endothelial growth factor (VEGF) in endothelial cells and prevents the diabetes-

induced increase in VEGF, thus inhibiting angiogenesis in diabetic retinopathy [14]. Chemokine CCL5 (formerly RANTES) of the CC-chemokine family, which plays a critical role in local invasion and distant metastasis in chondrosarcoma, promotes VEGF expression and angiogenesis by downregulating miR200b [15]. miR-200c radiosensitized the lung cancer cell line A549 by targeting the VEGF-VEGFR2 pathway [16]. From these reports, we speculated that the overexpression of the miR-200 family can regulate the expression and secretion of cytokines and growth factors involving in cell growth and migratory and invasive abilities of TNBC cells.

In the present study, we used MDA-MB-231 cells, a typical human TNBC cell line, which were stably transduced with lentivirus. We found that the overexpression of the miR-141/200c cluster promoted stronger migration and invasion of, as well as VEGF-A secretion by MDA-MB-231 cells. Therefore, we investigated, in detail, the mechanisms by which two miR-200 family members, the miR-200b/200a/429 cluster and the miR-141/200c cluster, regulated MDA-MB-231 cell migration and invasion. We demonstrate that the overexpression of the miR-141/200c cluster in MDA-MB-231 cells increased VEGF-A secretion, which enhanced the migratory ability of the cells through the activation of focal adhesion kinase (FAK) and the phosphatidylinositol-4,5-bisphosphate 3-kinase (PI3K)/protein

kinase B (AKT) signaling pathway.

MATERIALS AND METHODS

1. Cell culture

The human breast cancer cell lines MCF-7 (ER-positive subtype), MDA-MB-231 and HCC-38 (TN subtype) were obtained from the Korean Cell Line Bank (Seoul, Korea). Hs578T cells (TN subtype) were obtained from ATCC (Manassas, VA, USA). MCF-7 cells were grown in Dulbecco's Modified Eagle's Medium (DMEM) (WelGENE, Daegu, Korea) containing 10% fetal bovine serum (FBS) and supplemented with a 1% antibiotic solution containing penicillin and streptomycin (Gibco, Auckland, NZ). The MDA-MB-231, HCC-38, and Hs578T cells were grown in Roswell Park Memorial Institute (RPMI) 1640 medium (WelGENE) containing 10% FBS and supplemented with a 1% antibiotic solution containing penicillin and streptomycin (Gibco). The MCF-7, MDA-MB-231, HCC-38, and Hs578T cells used in this study were authenticated and validated by DNA fingerprinting (AmplFLSTR identifiler PCR Amplification kit), which was conducted by the Korean Cell Line Bank.

2. Lentiviral transduction

Viral vectors containing either the miR-200b/200a/429 cluster (GenBank ID: 406984 406983) or the miR-141/200c cluster

(GenBank ID: 406985 406933) constructs and the green fluorescent protein (GFP) construct were kindly supplied by Dr. Gregory J. Goodall of the University of Adelaide (Adelaide, Australia). A viral vector (pLenti M1.41) containing GFP was used as a control vector. Lentiviral transduction was conducted according to the manufacturer's instructions. Briefly, cells were seeded at a density of approximately 10-25% confluency (1×10^5 cells) in 6-well plates and were maintained at 37°C with 5% CO_2. Following an overnight culture, the culture medium was removed. Aliquots of the lentiviral stocks containing the miR-200b/200a/429 cluster or the miR-141/200c cluster construct as well as the control virus were gently mixed with 8 μg/ml polybrene and added to each well. After 6 hours of transduction, the medium was replaced with fresh complete medium. Transduced cells with a cell density of greater than 90% confluency were selected using medium containing 3 μg/ml puromycin for 2 weeks. Then, the GFP-positive cells were sorted from the selected cells using a FACSCalibur flow cytometer (BD Biosciences, Franklin Lakes, NJ, USA). Cancer cells stably expressing the miR-200b/200a/429 cluster or the miR-141/200c cluster and GFP, denoted as miR-200ab cells and miR-200c cells, respectively, and cancer cells containing the

pLenti M1.41 vector, denoted as control cells, were generated and expanded for use in all subsequent studies.

3. Quantitative real-time PCR

TaqMan MicroRNA Assays (Applied Biosystems, South San Francisco, CA, USA) were used to quantify the levels of mature miRNAs, following the manufacturer's instructions. The miRNAs were isolated from cells using the mirVana miRNA isolation kit (Applied Biosystems), and the specific primers for detecting miR-200a, miR-200b, and, miR-200c were purchased from Applied Biosystems. Reverse transcription was performed using the TaqMan microRNA reverse transcription kit (Applied Biosystems) according to the manufacturer's instructions. The traditional TaqMan Assay control, 18s rRNA, was used as the endogenous control. Each TaqMan Assay was conducted in triplicate.

4. Reverse transcriptase polymerase chain reaction (RT-PCR)

The total RNA was isolated using TRIzol Reagent (Invitrogen, Carlsbad, CA, USA) and reverse-transcribed using random hexamers and Superscript III reverse transcriptase. The cDNAs were synthesized using M-MLV reverse transcriptase (New England Biolabs, Ipswich, MA, USA) and random primers. The mRNA levels in the miR-200

family-transduced cells and non-transduced cells, referred to as the control, were evaluated using the conventional RT-PCR method with the following primer sets: E-cadherin (421 bp), F, ATTCTGATTCTGCTGCTCTTG and R, AGTAGTCATAGTCCTGGTCTT; Vimentin (247 bp), F, CCCTCACCTGTGAAGTGGAT and R, TCCAGCAGCTTCCTGTAGGT; ZEB1 (150 bp), F, TTCAAACCCATAGTGGTTGCT and R, TGGGAGATACCAAACCAACTG; ZEB2 (127 bp), F, CAAGAGGCGCAAACAAGC and R, GGTTGGCAATACCGTCATCC; Snail (557 bp), F, CAGACCCACTCAGATGTCAA and R, CATAGTTAGTCACACCTCGT; Fibronectin (171 bp), F, CAGAATCCAAGCGGAGAGAG and R, CATCCTCAGGGCTCGAGTAG; and β-actin (335 bp), F, TTCCTGGGCATGGAGTCCTGTGG, and R, CGCCTAGAAGCATTTGCGGTGG. Each target gene was amplified using a Thermocycler (BioRad, Hercules, CA, USA). The PCR products were subjected to electrophoresis through 1.5% agarose gels, and the levels of gene expression were normalized to that of β-actin.

5. Cell viability and proliferation assay

In vitro cell viability and proliferation were assessed using the 3-(4, 5-dimethylthiazol-2-yl)-2,5-diphenyl tetrazolium bromide (MTT) assay. Briefly, 5×10^3 cells were allowed to adhere in a high-humidity

environment in 5% CO_2 at 37°C in 96-well culture plates. At 1 d, 3 d, and 5 d after cell seeding, the MTT solution (a final concentration of 1 mg/ml) was added, and the cells were incubated for 1 h. At the end of the incubation period, the MTT solution was carefully removed, and 150 μl of dimethyl sulfoxide was added to each well. The plates were maintained on a rocker shaker for 10 min at 25°C, and then the amount of MTT formazan crystals formed by the viable cells was determined using a spectrophotometer based on the absorbance at 540 nm (GE Healthcare, Piscataway, NJ, USA). Flow cytometry analysis using 7-AAD was performed to confirm cell viability.

6. Migration and invasion assay

To assess the cell migratory ability, $2-5 \times 10^4$ cells were suspended in 100 μl of medium with or without 10% FBS and deposited in the upper chambers of a trans-well plate with 8.0-μm pores (BD Biosciences) with a non-coated membrane. For the invasion assays, 5×10^4 cells were plated in 2% Matrigel™ (BD Biosciences) basement membrane matrix-coated upper chambers in a trans-well plate with 8.0-μm pores. The lower chambers were filled with 600 μl of medium supplemented with 10% FBS, and the cells were incubated for 48 h at

37°C in the presence or absence of an FAK inhibitor (5 μM PF573228, Sigma, St. Louis, MO, USA), a PI3K/AKT inhibitor (20 μM LY294002, Cell Signaling Technology, Danvers, MA, USA), 5 μg/ml VEGF-neutralizing antibody (Santa Cruz Biotechnology, Dallas, TX, USA) or 10 ng/ml VEGF-A protein (Sigma). Each inhibitor, VEGF-neutralizing antibody, or VEGF-A were added in both the upper and lower chambers. No chemoattractants were used in the lower chamber for either the migration or invasion assays. The cells that migrated from the upper chamber were stained using a crystal violet solution (0.5% crystal violet in 20% methanol) for 5 min. Unbound crystal violet was removed by rinsing using distilled water. The cells were subsequently air-dried, and the crystal violet was eluted from the cells using a solution of 1% sodium dodecyl sulfate (SDS). The absorbance of crystal violet at 550 nm was measured using a spectrophotometer (GE Healthcare).

7. Wound-healing assay

Cells were seeded at 5×10^4 cells per well in six-well plates and cultured under permissive conditions until reaching 90% confluence. After 24 h, each confluent cell monolayer was lightly and quickly scratched using a sterile plastic tip to produce a straight line. The

debris was removed, and the edge of the scratch was smoothed by washing with PBS. The cells were cultured for 6 h in complete medium, after which, the lateral migratory activity was evaluated based on the area occupied by the cells that had entered the scratch line at 0 h. Images were acquired using a microscope (Leica, Wetzlar, Germany) equipped with a CCD camera (Leica). The migration rates were calculated according to the equation percentage wound healing = [(wound length at 0 h) − (wound length at 6 h)] / (wound length at 0 h) × 100. The mean results of three straight distances (upper edge, middle, and lower edge) in scratch area were evaluated as wound lengths. Length quantification was performed using ImageJ software (NIH, Bethesda, MD, USA).

8. Measurement of cytokines and growth factors

Samples of 1−2 × 10^5 cells were seeded in 6−well plates. After a two−day culture period, when cells were at 90% confluency, the conditioned medium was harvested. The levels of secreted cytokines and growth factor (IL−2, IL−4, IL−5, IL−10, IL−12, IL−13, GM−CSF, IFN−γ, and VEGF−A) were quantified using the Bio−Plex200 multiplex array system according to the recommended protocol (Bio−Rad). All samples and standardized solutions were analyzed in triplicate.

9. Western blotting

The cells were lysed in RIPA buffer (Sigma). The proteins were separated using SDS-polyacrylamide gel electrophoresis and were transferred to nitrocellulose membranes. The membranes were blocked using 5% skim milk in Tris-buffered saline containing Tween and incubated with primary antibodies directed against ERK, phospho-ERK, AKT (anti-rabbit polyclonal antibody, Cell Signaling Technology), phospho-AKT (anti-mouse polyclonal antibody, Cell Signaling Technology), FAK (anti-rabbit polyclonal antibody, Invitrogen), phospho-FAK (anti-rabbit polyclonal antibody, Invitrogen), integrin-αV (anti-rabbit polyclonal antibody, Santa Cruz Biotechnology) or β-actin (anti-mouse polyclonal antibody, Sigma) overnight at 4°C. The membranes were then incubated with horseradish peroxidase-conjugated secondary antibodies (Santa Cruz Biotechnology). The blotted membranes were visualized using enhanced chemiluminescence reagents (GE Healthcare). Western blot quantification was performed using ImageJ software.

10. Immunofluorescence staining

The cells were seeded on sterile cover slips in 24-well plates. Then, the cells were fixed using a 4% paraformaldehyde solution (Affymetrix,

Cleveland, OH, USA). Primary antibodies directed against integrin-αV (Santa Cruz Biotechnology) and phospho-FAK (Invitrogen) were applied overnight at 4°C. The bound integrin-αV and phospho-FAK antibodies were visualized using secondary antibodies conjugated to Alexa 594, and the nuclei were counterstained using 4',6-diamidino-2-phenylindole (DAPI). All multicolor fluorescence images were obtained using a confocal laser-scanning microscopy (LSM5 Meta) (Carl Zeiss, Oberkochen, Germany).

11. Statistical analyses

For the entire dataset obtained in this study, the mean values ± standard deviations were calculated from the results of at least three independent experiments and were statistically evaluated using a one-way ANOVA followed by the t-test. For all tests, p-values of less than 0.05 were considered significant.

RESULTS

Overexpression of the miR-200b/200a/429 cluster or the miR-141/200c cluster enhanced the migratory and invasive abilities of MDA-MB-231 cells

We first investigated alterations in the characteristics of two different breast cancer cell lines, MCF-7 and MDA-MB-231 cells, caused by the stable transduction of constructs encoding miR-200 family members and GFP using lentiviruses. The GFP-positive cells comprised more than 95% of the miR-200b/200a/429 cluster- or miR-141/200c cluster-transduced MCF-7 and MDA-MB-231 cells (Figure 1-1 and 1-2). Strong GFP expression in the miR-200b/200a/429 cluster- or miR-141/200c cluster-transduced MCF-7 and MDA-MB-231 cells was evaluated using microscopy (Figure 1-1A and 1-3A). RT-PCR was used to evaluate expression levels of EMT markers, and the results showed that the overexpression of the miR-200b/200a/429 cluster or the miR-141/200c cluster resulted in the induction of E-cadherin expression and a decrease in ZEB-1 expression in MDA-MB-231 cells (Figure 1-1B). Overexpression of the miR-200ab or miR-200c cluster led to increased expression of Snail in MCF-7 and MDA-MB-231 cells.

To investigate the stable overexpression of miR-200a, miR-200b,

miR-200c in miR-200b/200a/429 cluster- or miR-141/200c cluster-transduced MDA-MB-231 cells, real-time RT-PCR was conducted to quantify the levels of the mature microRNAs. As expected, the miR-200b/200a/429 cluster- and miR-141/200c cluster-transduced MDA-MB-231 cells showed increased mature miR-200a, miR-200b, and miR-200c levels at 5-100-fold higher levels than did the control MDA-MB-231 cells, which exhibited undetectable levels of all members of the miR-200 family (Figure 1-3B).

To investigate whether overexpression of the miR-200b/200a/429 or miR-141/200c cluster affected cell growth, an MTT assay was performed. Figure 3C shows that the growth rate of the miR-200b/200a/429 cluster- or miR-141/200c cluster-transduced MDA-MB-231 cells was similar to that of the control cells on the 3rd day but was significantly decreased on the 5th day after cell seeding compared with that of the control cells (control vs. miR-200ab, $P = 0.02$ and control vs. miR-200c, $P = 0.0002$) (Figure 1-3C). The overexpression of the miR-141/200c cluster was found to more strongly suppress the growth of MDA-MB-231 cells.

We assessed migratory and invasive abilities using a trans-well migration assay and a wound-healing assay. The results of crystal violet staining showed that the migratory ability of MCF-7 cells was suppressed by transduction of the miR-200 family, but there was no

significant difference between that of the miR-200b/200a/429 cluster- or miR-141/200c cluster-transduced MCF-7 cells and control cells (Figure 1-1C and 1-1E). The wound-healing assay, which demonstrated the lateral migratory ability of MCF-7 cells, yielded results similar to those of the trans-well migration assay (Figure 1-1D and 1-1F).

With regard to the trans-well migration and invasion assays of the miR-200b/200a/429 cluster- or miR-141/200c cluster-transduced MDA-MB-231 cells, after 48 h of incubation without an FBS gradient, cell migration significantly increased up to 1.94±0.22-fold and 2.49±0.08-fold in miR-200b/200a/429 cluster- or miR-141/200c cluster-transduced MDA-MB-231 cells, respectively, compared with control cells (Figure 1-3D control vs. miR-200ab, P = 0.04 and control vs. miR-200c, P = 0.002). To further investigate the migratory ability of miR-141/200c cluster-transduced MDA-MB-231 cells, the trans-well migration assay under the condition of a 10% FBS gradient in the upper (0% FBS) and the lower chamber (10% FBS) was conducted for 24 h. A significant increase was observed in the migratory ability of the miR-141/200c-transduced MDA-MB-231 cells (1.53±0.30-fold) relative to MDA-MB-231 cells (Figure 1-4, p=0.0009). As expected, the results of an invasion assay using

Matrigel™ matrix-coated trans-well membranes showed a significant increase in the invasive ability of the miR-200b/200a/429 cluster-transduced cells (1.61±0.31-fold) and miR-141/200c cluster-transduced cells (1.98±0.40-fold) after 48 h of incubation compared with that of control cells (Figure 1-3E, control vs. miR-200ab, P = 0.0005 and control vs. miR-200c, P = 0.0002). The elevated migration and invasion rates were higher in miR-141/200c cluster-transduced MDA-MB-231 cells than miR-200b/200a/429 cluster-transduced MDA-MB-231 cells. After 6 h of incubation, the transduction of miR-200b/200a/429 cluster or miR-141/200c cluster did not affect the lateral migratory ability of MCF-7 cells, but increased the lateral migration up to 2.78±0.11-fold and 1.69±0.11-fold in miR-200b/200a/429 cluster- or miR-141/200c cluster-transduced MDA-MB-231 cells, respectively (P = 0.02, Figure 1-1F). In other TNBC cell lines, HCC-38 and Hs578T cells, we observed a significant increase in trans-well migration ability in both the miR-141/200c cluster-transduced HCC-38 cells (1.64±0.11-fold, P < 0.001) and miR-141/200c cluster-transduced Hs578T cells (1.76±0.44-fold, P = 0.0003) compared with the control cells (Figure 1-5A and D). The mature miR-200c levels in miR-141/200c cluster-transduced HCC-38 and Hs578T cells were 252- and 205-fold higher than that in the

control HCC-38 and Hs578T cells, which exhibited undetectable levels of miR-200c ($P < 0.001$, Figure 1-6G and H).

We found that the overexpression of the miR-200b/200a/429 cluster or the miR-141/200c cluster resulted in the highest migratory capacity in MDA-MB-231 cells compared with the other TNBC cells, HCC-38 and Hs578T cells. Therefore, we focused on the regulatory mechanisms by which the miR-200b/200a/429 cluster or the miR-141/200c cluster promoted the migratory and invasive capacities of the MDA-MB-231 cell line, as a representative TNBC cell line.

Overexpression of the miR-200b/200a/429 cluster or the miR-141/200c cluster enhanced the phosphorylation of FAK and AKT and the expression of integrin in MDA-MB-231 cells

We investigated whether the overexpression of miR-200 family members modulated the focal adhesion kinase (FAK), PI3K/AKT, and MEK/ERK signaling pathways, which are involved in cell proliferation and migration. Representative western blotting results showed that the levels of FAK and AKT phosphorylation were greatly increased, but the level of ERK phosphorylation was not significantly changed in the miR-200b/200a/429 cluster- or miR-141/200c cluster-transduced MDA-MB-231 cells (Figure 1-7A, left). The level of phosphorylated FAK was significantly increased up to 1.52±0.26-fold and 3.12±1.56-

fold in the miR-200b/200a/429 cluster-transduced cells and miR-141/200c cluster-transduced cells, respectively (Figure 1-7A, right, control vs. miR-200ab, P = 0.01 and control vs. miR-200c, P = 0.09). The level of phosphorylated AKT was also increased 2.21±1.06-fold and 9.32±11.07-fold in the miR-200b/200a/429 cluster-transduced cells and miR-141/200c cluster-transduced cells, respectively (Figure 1-7A, right, control vs. miR-200ab, P = 0.19 and control vs. miR-200c, P = 0.32). We also observed that the miR-141/200c cluster significantly increased the phosphorylation levels of FAK (1.98±0.37-fold, P = 0.04) and AKT (5.61±1.73-fold, P = 0.04) in HCC-38 cells (Figure 1-8C and D). Representative western blotting results showed that the expression levels of integrin-αV, which is associated with the FAK signaling pathway, were increased in both the miR-200b/200a/429 cluster- and miR-141/200c cluster-transduced cells (Figure 1-7B, left). Integrin-αV expression was increased 1.57±0.10-fold and 1.70±0.24-fold in the miR-200b/200a/429 cluster-transduced cells and miR-141/200c cluster-transduced cells, respectively (Figure 1-7B, right, control vs. miR-200ab, P = 0.01 and control vs. miR-200c, P = 0.04). Integrin-αV expression was also increased (13.61±0.72-fold, P = 0.008) in miR-141/200c cluster-

transduced HCC-38 cells (Figure 1-8C and D). To investigate the cellular localization of phosphorylated FAK and integrin-αV, immunofluorescent staining was assessed. Phosphorylated FAK was largely localized at the focal adhesions of the plasma membranes of the miR-200b/200a/429 cluster- and miR-141/200c cluster-transduced cells (Figure 1-7C). Integrin-αV accumulated and clustered at the periphery of the plasma membranes of the miR-200b/200a/429- and miR-141/200c-transduced cells compared with that in control cells (Figure 1-7C). The levels of FAK phosphorylation and integrin-αV expression were higher in the miR-141/200c cluster-transduced HCC-38 cells than in the control cells (Figure 1-8E).

To determine the signaling pathway involved in enhanced migratory and invasive ability of miR-200b/200a/429 cluster- or miR-141/200c cluster-transduced MDA-MB-231 cells trans-well migration assays were performed in the presence of PF573228 or LY294002, which are chemical inhibitors of FAK and PI3K/AKT, respectively. The chemical inhibitors were added to both the upper and lower chambers, which would allow their effects to last throughout the entire experimental period. The enhanced migratory activity was completely inhibited in miR-200b/200a/429 cluster- and miR-141/200c cluster-transduced MDA-MB-231 cells treated with the

FAK or PI3K/AKT inhibitor, reaching the basal migratory level of MDA-MB-231 cells (Figure 1-7D). These observations demonstrated that the elevated migratory ability of MDA-MB-231 cells by stable overexpression of miR-200b/200a/429 cluster or miR141/200c cluster was driven by the activation of the FAK and PI3K/AKT-mediated signaling pathways.

Overexpression of the miR-200b/200a/429 cluster or the miR-141/200c cluster increased the level of VEGF-A secretion in MDA-MB-231 cells

The secreted cytokines or growth factors that might be involved in regulating the migration of the miR-200b/200a/429 cluster- or miR141/200c cluster-transduced cells were analyzed. The levels of IL-2, GM-CSF, and IFN-γ secreted into the medium by the miR-200b/200a/429 cluster- and miR-141/200c cluster-transduced MDA-MB-231 cells after 48 h of culture were lower than those of the control MDA-MB-231 cells. However, the secreted VEGF-A levels were significantly higher in the conditioned medium of the miR-200b/200a/429 cluster-transduced cells (1.64±0.03-fold) and miR-141/200c cluster-transduced cells (2.66±0.09-fold) than in that of the control MDA-MB-231 cells (Figure 1-9A, control vs. miR-200ab, $P = 0.007$ and control vs. miR-200c, $P = 0.0007$). Increased secretion

of VEGF-A was higher in miR-141/200c cluster-transduced cells than miR-200b/200a/429 cluster-transduced cells (miR-200ab vs. miR-200c, P = 0.0001). The secreted levels of cytokines and growth factors were also evaluated in the miR-141/200c cluster-transduced HCC-38 and Hs578T cells. VEGF-A secretions were significantly increased in miR-141/200c cluster-transduced HCC-38 (1.75±0.03-fold, P = 0.00001) and miR-141/200c cluster-transduced Hs578T cells (1.17±0.16-fold, P = 0.004) relative to control cells (Figure 1-5B and E). The effect of miR-141/200c overexpression on increased cell migration and VEGF-A secretion was greater in MDA-MB-231 cells relative to HCC-38 and Hs578T cells. There were no definite differences in VEGF-A secretion levels between the miR-141/200c cluster-transduced Hs578T and the control Hs578T cells. These results were explained by the phenotypic and functional heterogeneity among cancer cells in TNBC cells. The VEGF-A expression levels were also examined in the miR-200b/200a/429 cluster- or miR141/200c cluster-transduced MDA-MB-231 cells, but the transduction of miR-200b/200a/429 cluster (1.18±0.31-fold) or miR-141/200c cluster (0.90±0.34-fold) did not affect VEGF-A expression (Figure 9B, right, control vs. miR-200ab, P = 0.38 and control vs. miR-200c, P = 0.45). The miR-141/200c cluster-transduced HCC-38

cells (0.92±0.09-fold) also expressed VEGF-A levels that were similar to the control HCC-38 cells (Figure 1-8A, P = 0.46).

Blocking VEGF-A activity inhibited the enhanced migration and invasion of miR-200b/200a/429 cluster or miR-141/200c cluster-transduced MDA-MB-231 cells

To examine whether secreted VEGF-A regulates the migratory and invasive abilities of the miR-200b/200a/429 cluster- or miR141/200c cluster-transduced MDA-MB-231 cells, trans-well migration and invasion assays were performed after treatment with anti-VEGF-A-neutralizing antibodies. The anti-VEGF-A-neutralizing antibodies were added to both the upper and lower chamber, which would allow their effects to last throughout the entire experimental period. Figures 1-9C and D showed that the anti-VEGF-A-neutralizing antibodies completely inhibited the increased migratory (control vs. miR-200ab, P = 0.0001 and control vs. miR-200c, P = 0.002) and invasive (control vs. miR-200ab, P = 0.02 and control vs. miR-200c, P = 0.001) abilities of the miR-200b/200a/429 cluster- and miR-141/200c cluster-transduced cells. These data clearly indicated that secreted VEGF-A was involved in promoting the migration and invasion of both miR-200b/200a/429 cluster- and miR141/200c cluster-transduced cells. The administration of anti-VEGF-A-antibodies for neutralizing VEGF-A in cultured medium suppressed the

migration increased by miR-141/200c overexpression in both the miR-141/200c cluster-transduced HCC-38 and miR-141/200c cluster-transduced Hs578T cells (Figure 1-5C and F). The anti-VEGF-A-neutralizing antibodies also completely inhibited the increased migratory ability (control vs. miR-200c, $P < 0.001$) of the miR-141/200c cluster-transduced HCC-38 cells (Figure 1-5C, untreated vs. VEGF-A Ab, $P < 0.001$).

These results supported that VEGF-A secretion was associated with enhancing migration ability in TNBC cells. The anti-VEGF-A-neutralizing antibodies partly blocked the enhanced migratory ability (control vs. miR-200c, untreated, 1.76±0.44-fold, $P = 0.0003$) of both the control (0.80±0.07-fold, $P = 0.003$) and the miR-141/200c cluster-transduced Hs578T cells (1.37±0.21-fold, $P = 0.003$), but the miR-141/200c cluster-transduced Hs578T cells still showed increased migratory ability compared with that of the control cells (control vs. miR-200c, VEGF-A Ab treated, $P < 0.001$, Figure 1-5F). These results imply that other factors besides VEGF-A may also be involved in promoting migration in miR-141/200c cluster-transduced Hs578T cells.

The miR-141/200c cluster activated the FAK and PI3K/AKT signaling pathway by secreted VEGF-A, resulting in the promotion of the

migratory and invasive abilities of MDA-MB-231 cells

To ascertain the VEGF-A-mediated intracellular signaling pathway responsible for the increased migratory and invasive abilities of miR-200b/200a/429 cluster- or miR141/200c cluster-transduced MDA-MB-231 cells, the levels of FAK and AKT phosphorylation were evaluated in cells treated with 5 μg/ml anti-VEGF-A-neutralizing antibodies. Treatment with anti-VEGF-A-neutralizing antibodies for both 30 min and 48 h remarkably decreased the level of FAK and AKT phosphorylation in the miR-141/200c cluster-transduced MDA-MB-231 cells and the control cells but did not affect the level of phosphorylated FAK and AKT in the miR-200ab cluster-transduced MDA-MB-231 cells (Figure 1-9E and F). In contrast, the level of ERK phosphorylation was increased by anti-VEGF-A-neutralizing antibodies in miR-141/200c-transduced cells and control cells. These data implied that FAK and AKT acted as a direct link between elevated VEGF-A secretion and the consequential signal transduction related to enhanced migration of miR-141/200c cluster-transduced MDA-MB-231 cells, but the increased secretion of VEGF-A in miR-200b/200a/429 cluster-transduced MDA-MB-231 cells was not directly followed by activation of the FAK and AKT-mediated signaling pathway, which was possibly induced by the other signaling pathways.

Exogenous VEGF-A stimulated migration of MDA-MB-231 cells by activating the FAK and PI3K/AKT pathway

To confirm the role of VEGF-A as a migration-activating mediator in miR-200b/200a/429 cluster- or miR-141/200c cluster-transduced MDA-MB-231 cells, a trans-well migration assay was assessed in MCF-7 and MDA-MB-231 cells treated with exogenous VEGF-A protein. The representative crystal violet staining of exogenous VEGF-A (10 ng/ml)-treated MCF-7 and MDA-MB-231 cells that had migrated through the trans-well membranes after 48 h is shown in Figure 1-10A. A quantitative analysis of a crystal violet assay showed that exogenous VEGF-A significantly increased MDA-MB-231 cell migration up to 1.50±0.16-fold but had no effect on the migratory ability of MCF-7 cells compared with that of untreated cells (Figure 1-10B, untreated vs. VEGF-A, $P = 0.003$). In addition, we investigated whether VEGF-A played a role as a migration-activating mediator in HCC-38 cells. As expected, VEGF-A treatment significantly increased HCC-38 cell migration up to 1.56±0.26-fold (Figure 1-11B, untreated vs. VEGF-A, $P < 0.001$).

To verify the exogenous VEGF-A-mediated intracellular signaling pathways responsible for the increased migratory ability of MDA-MB-231 cells, the levels of FAK, AKT, and ERK phosphorylation were

evaluated. After cell starvation for 4 h, treatment with exogenous VEGF-A for 15 min, 30 min, 60 min, and 48 h induced the periodic fluctuation of the phosphorylation levels of FAK and AKT and generally increased phosphorylated FAK and AKT, but did not affect the phosphorylation level of ERK in MDA-MB-231 cells (Figure 1-10C and D). These data indicated that the activation of the FAK and PI3K/AKT signaling pathways mediated by the exogenous VEGF-A increased the migratory ability of MDA-MB-231 cells. Similar results that VEGF-A stimulated FAK, AKT, and ERK were also observed in HCC-38 cells (Figure 1-11C and D).

DISCUSSION

The role of miR-200 family in regulating the migration and invasion of different cancer cell types is controversial [10, 11]. Moreover, only a small number of miR-200 target genes that regulate cell migration and cancer metastasis has been identified [4, 6], and the mechanisms underlying the functions of miR-200b/200a/429 cluster and miR-141/200c cluster in TNBC cells are not fully understood. It is well-known that the miR-200 family expression levels are significantly lower in highly migratory TNBC cells and metastatic TNBC tumors than other types of breast cancer cells and tumors. In addition, Vrba L *et al.* reported that the repression of miR-200 and miR-141 expression due to aberrant epigenetic gene silencing in aggressive cancer cells, including MDA-MB-231 cells, indicating that the downregulation of miR-200 may contribute to an aggressive TNBC phenotype [17]. ZEB1 and SIP1 have been found to repress primary transcript and mature miR-200 expression in mesenchymal types of breast cancer cells, suggesting a downregulation of miR-200 in TNBC cells through a potential double-negative feedback loop between ZEB1/SIP1 and the miR-200 family [18]. Manav K *et al.* reported the highest expression of miR-200s in the highly metastatic 4T1 cells, a mouse TNBC cell line, which was consistent with acquisition of epithelial traits in 4T1 cells compared with the weakly metastatic

4TO7 cells. In addition, 4T1 tumors exhibit spontaneous metastasis and colonization of distant organs, which is enhanced by miR-200 overexpression in experimental animal models; furthermore, higher expression of miR-200 levels were found in lung-pleural metastasis samples relative to primary tumor samples in breast cancer patients. These data support the potential role of miR-200s in migration, invasion, metastatic colonization, and metastatic dissemination [6]. Recently, Avery-Kiejda KA *et al.* found that the miR-200 cluster is upregulated in invasive ductal carcinomas with both lymph node-positive and lymph node-negative TNBC compared with matched normal adjacent tissues [19]. Their reports of *in vivo* experimental and clinical evidence may indicate that tumor cell populations with increased aggressiveness may have higher miR-200 cluster levels than their less aggressive counterparts within the same TNBC and in normal tissues; the miR-200 cluster, though being generally reduced in TNBC compared with other subtypes, is upregulated in TNBC cells that may support metastatic dissemination. We showed here that the overexpression of miR-200b/200a/429 cluster or miR-141/200c cluster strongly promoted the migration and invasion of MDA-MB-231, HCC-38, and Hs578T cells, typical claudin-low and mesenchymal subtypes of TNBC cell lines [20], compared with those of an ER-positive breast cancer cell line, MCF-7 cells. The migratory and invasive ability of MDA-MB-231 cells was substantially more

enhanced in those that overexpressed the miR-141/200c cluster than in those with the miR-200b/200a/429 cluster. These data suggest that the different roles of the miR-200 family members, such as miR-200a, miR-200b, miR-200c, miR-141, and miR-429, on the migration and invasion of different subtypes of human breast cancer cell lines classified by molecular characterization should be further investigated [21].

Dysregulation of the PI3K/AKT signaling pathway has been implicated in mammary carcinogenesis and was suggested to be the mechanism underlying the survival of invasive breast cancer cells [22]. Furthermore, an activated AKT signaling pathway, a common dysregulation observed in breast cancers, has been shown to promote cancer cell growth, survival, and metastasis [23]. FAK is a cytoplasmic tyrosine kinase that plays crucial roles in integrin-mediated signal transduction, and FAK localizes to the sites where transmembrane integrin receptors are clustered to mediate various intracellular signal-transduction pathways [5, 24]. Many recent studies have reported that an increased level of FAK expression highly correlates with the invasiveness and metastasis of human tumors [25-27]. We found that the phosphorylation levels of AKT and FAK in MDA-MB-231 cells were elevated by stable overexpression of the miR-200b/200a/429 cluster and the miR-141/200c cluster. Additionally, increased

integrin-αV and phosphorylated FAK co-localized in the transmembrane of miR-200b/200a/429 cluster- and miR-141/200c cluster-transduced MDA-MB-231 cells. These data suggest that the stable overexpression of the 200b/200a/429 cluster and the miR-141/200c cluster in MDA-MB-231 cells may affect the secretion of cytokines or growth factors to activate FAK or the PI3K/AKT signaling pathway. The regulation between the miR-200 family and FAK is not fully understood. A model indicating that a stiffer matrix of breast cancers will activate FAK, which inhibits the miR-200 family and allow for a mesenchymal phenotype has been proposed [28]. This model is not consistent with our observation that the overexpression of the miR141/200c cluster or the miR-200b/200a/429 cluster increased clustering and expression of integrins and activated FAK and AKT, which regulate cell migration. Our finding proposes a positive cross-talk between FAK and overexpressed miR-200 in TNBC cells.

Many studies have been aimed at understanding the role of cytokines and growth factors in breast cancer progression. Some cytokines and growth factors (IL-1, IL-6, IL-11, TGF- β, and VEGF) stimulate the proliferation and invasion of breast cancer cells, whereas others (IL-12, IL-18, and IFN) suppress breast cancer progression [29]. A recent study reported that miR-200 inhibits angiogenesis by targeting IL-8 and CXCL1 secreted by tumor endothelial and cancer

cells [30]. Our study demonstrated that the overexpression of the miR-200b/200a/429 cluster or the miR-141/200c cluster in MDA-MB-231 cells led to a decrease in the secretion of IL-2, IL-4, IL-5, IL-10, IL-13, GM-CSF, INF-γ and TNF-α but a significant increase in the secretion of VEGF-A. VEGF has been reported to activate the PI3K/AKT/forkhead signaling pathway to promote angiogenesis in human endothelial cells [31]. In addition, VEGF-A, the most potent angiogenic factor in tumor angiogenesis, induces oligodendrocyte precursor cell migration through a ROS- and FAK-dependent mechanism [32]. VEGF-A is known to be a direct target of miR-200b [33], but in our results, a significant decrease in VEGF-A levels assessed by western blotting was not observed in miR-200b/200a/429- and miR-141/200c-transduced MDA-MB-231 cells or in miR-141/200c-transduced HCC-38 cells relative to control. Moreover, VEGF-A secretions in MDA-MB-231, HCC-38, and Hs578T cells were increased by the overexpression of the miR-141/200c cluster. The comprehensive interactions between miRNAs and transcription factors (TFs) are expected to comprise "wired" genetic networks to regulate the expression of target genes [34]. In examples of an incoherent feed-forward loop, the direct regulatory effect of TFs on the target gene (VEGF-A) is opposed to the indirect regulatory effect through miR-200 regulation. Taking the

comprehensive interactions between miRNAs and protein-coding genes, we propose that miR-200 overexpression in TNBC cells can affect TFs (HIF-1, CREB) or signals (PI3K/AKT) to regulate VEGF-A secretion through an incoherent feed-forward loop. An autocrine loop for VEGF-A to induce breast cancer cell migration/invasion has been well documented [35, 36]. From these reports, we assume that the VEGF-A secreted by miR-200 overexpression interacts with its receptors, such as neuropilin-1 (NP-1) and VEGFR, and stimulates the PI3K/AKT signaling pathway, thus promoting TNBC cell migration and invasion. In this study, we demonstrated that treatment with VEGF-A led to an increase in migratory ability and activated FAK and the PI3K/AKT signaling pathway in MDA-MB-231 cells and HCC-38 cells. Our results strongly support that VEGF-A-mediated FAK or PI3K/AKT signaling pathway modulates cancer cell migration and invasion. By down-regulating miR-200b expression through the PI3K/AKT signaling pathway, the chemokine CCL5 (formerly RANTES) promotes VEGF-dependent angiogenesis in human chondrosarcomas [15]. In addition, synthetic miR-200c downregulates VEGF-A by the direct targeting of the 3'UTR of VEGF-A mRNA in a lung cancer cell line [16]. Contrary to above studies, in this study, the stable overexpression of the miR-200b/200a/429 cluster and the miR-141/200c cluster in MDA-MB-231 cells resulted in increased VEGF-A secretion and induced AKT and FAK phosphorylation. Blocking the

PI3K/AKT or FAK signaling pathways using chemical inhibitors inhibited the enhanced migration and invasion in MDA-MB-231 cells overexpressing the miR-200b/200a/429 cluster or the miR-141/200c cluster. Inhibiting the VEGF-A-mediated pathway using anti-VEGF-A-neutralizing antibodies suppressed the elevated AKT and FAK phosphorylation in MDA-MB-231 cells overexpressing miR-141/200c cluster, reversing the enhanced migratory and invasive abilities. These results suggest that the activation of FAK and the PI3K/AKT signaling pathway are directly mediated by elevated VEGF-A secretion, which is involved in the increased migratory and invasive abilities of miR-141/200c cluster-transduced MDA-MB-231 cells. On the other hand, FAK- and PI3K/AKT-independent signaling pathways activated by VEGF-A may lead to an enhanced migratory ability in miR-200b/200a/429 cluster-transduced MDA-MB-231 cells. The present study implies that aberrant expression of miR-200b/200a/429 cluster or the miR-141/200c cluster may play a pro-metastasis role leading to the promotion of migration and invasion of MDA-MB-231 cells.

Chapter 2

LOXL4 knockdown enhances tumor growth and lung metastasis through collagen-dependent extracellular matrix changes in triple-negative breast cancer

INTRODUCTION

Elevated collagen deposition and alterations in the structure of the extracellular matrix (ECM) are common in various forms of cancer [37, 38]. In particular, elevated expression and deposition of collagen I and IV affects laminin levels and has been implicated in abnormal stiffness of the ECM [39]. Aberrant expression of lysyl oxidase (LOX) family genes, which catalyze collagen cross-link formation, and of the procollagen-lysine 2-oxyglutarate 5-dioxygenase (PLOD) and prolyl 4-hydroxylase α subunit (P4HA) genes, which mediate collagen lysine hydroxylation, also alter the structure of the ECM [40-46].

Levels of lysyl oxidase-like 4 (LOXL4) are much lower than levels of other LOX family members in various normal tissues [47]. In addition, the associations between aberrant LOXL4 expression and its pathophysiological effects in cancer are similar to those observed for other LOX family members [48-53]. However, previous reports have obtained conflicting results regarding the effects of LOXL4 in cancer. In bladder cancer, LOXL4 suppresses tumors by inhibiting the oncogenic signaling pathway [52]. In contrast, LOXL4 promotes aggressive tumor progression and metastasis in colorectal and oral cancers [53, 54]. In breast cancer, LOXL4, LOX, and LOXL2, which are expressed in a hypoxia-inducible factor 1-dependent manner, recruit

bone marrow-derived cells and facilitate colonization of the lungs [55]. These conflicting results might be explained by differences in the cellular context among cancers that might influence whether LOXL4 acts as a tumor suppressor or a metastasis promoter. Although many studies have been conducted to elucidate the role of LOXL4 in cancer, the precise mechanisms by which LOXL4 suppresses tumors or promotes metastasis in breast cancer remain largely unknown. Clinical studies have shown that high LOX and LOXL2 expression are correlated with increased metastasis and poor survival in triple negative breast cancer (TNBC) patients [56, 57]. Interestingly, a recent report revealed that, among the LOX family members, LOXL4 mRNA levels alone were higher in cancer tissues from TNBC patients than in those from estrogen receptor-positive breast cancer patients [58]. Although these reports suggest that LOXL4 expression might affect clinical outcomes in TNBC patients, to the best of our knowledge, no studies have directly examined this relationship. Here, we injected mice with LOXL4-knockdown MDA-MB-231 cells, which are aggressive TNBC cells, to investigate the roles of LOXL4 in primary tumor growth and metastasis in a xenograft model. In addition, we evaluated the clinical significance of LOXL4 in human breast cancer patients using a public database with overall survival (OS) information.

MATERIALS AND METHODS

1. Cell lines

The human breast cancer cell lines MCF-7, BT-474, MDA-MB-453, SK-BR3, HCC1954, BT-549, MDA-MB-157, MDA-MB-231, MDA-MB-468, and HCC1937, and normal breast epithelial cells MCF-10A, were obtained from ATCC (Manassas, VA, USA) or the Korean Cell Line Bank (Seoul, Korea). The breast cancer cells used in this study were authenticated and validated by DNA fingerprinting (AmpFLSTR identifier PCR Amplification kit), which was conducted by the Korean Cell Line Bank or provided by the distributors.

2. Lentiviral transduction

Viral vectors containing either the TRIPZ-inducible lentiviral non-silencing shRNA control as a negative control vector or a TRIPZ-inducible LOXL4 shRNA (shLOXL4: clone ID V2THS_138014) construct and the red fluorescent protein (RFP) construct were purchased from GE Dharmacon (Pittsburgh, PA, USA). Lentiviral transduction was conducted according to the manufacturer's instructions. RFP-positive cells were selected from cultures maintained in medium containing 0.5-3 μg/mL puromycin for 2 weeks; selected cells were then sorted using a FACSCalibur flow cytometer

(BD Biosciences, Franklin Lakes, NJ, USA) and cultured in medium without puromycin. Cancer cells that stably expressed RFP and either the non-silencing shRNA or the LOXL4 shRNA, denoted control cells and shLOXL4 cells, respectively, were generated for use in all subsequent studies. Viral vectors containing the luciferase and green fluorescent protein (GFP) constructs were also transduced for the animal study using the same procedure described above. GFP-positive cells were then selected and sorted using a FACSCalibur flow cytometer.

3. RNA isolation and quantitative real-time PCR

Total RNA was isolated using TRIzol Reagent (Invitrogen, Carlsbad, CA, USA) and was reverse-transcribed using random hexamers and Superscript III reverse transcriptase. cDNAs were synthesized using M-MLV reverse transcriptase (New England Biolabs, Ipswich, MA, USA) and random primers. mRNA levels were measured in control and shLOXL4 cells using the quantitative real-time method and the following primer sets: LOX (174 bp) F, GTTCCAAGCTGGCTACTC, and R, GGGTTGTCGTCAGAGTAC; LOXL1 (244 bp) F, CAGACCCCAACTATGTGCAA, and R, ATGCTGTGGTAATGCTGGTG; LOXL2 (239 bp) F, GGAAAGCGTACAAGCCAGAG, and R, GCACTGGATCTCGTTGAGGT; LOXL3 (162 bp) F, ATGGGTGCTATCCACCTGAG, and R, GAGTCGGATCCTGGTCTCTG;

LOXL4 (165 bp) F, ACCGAAGACAAAGCCACAAC, and R, CACACGACACTGGCAGAGAT; and β-actin (335 bp) F, TTCCTGGGCATGGAGTCCTGTGG, and R, CGCCTAGAAGCATTTGCGGTGG. Relative gene expression was determined using an ABI 7500 real-time polymerase chain reaction (PCR) instrument (Applied Biosystems, South San Francisco, CA, USA) with pre-optimized conditions. PCR reactions were performed in triplicate. Expression ratios were calculated as the normalized threshold cycle (Ct) difference between the control and samples after adjustment for amplification efficiency relative to expression of the housekeeping gene β-actin.

4. Cell viability and proliferation assay

In vitro cell viability and proliferation were assessed using the 3-(4, 5-dimethylthiazol-2-yl)-2,5-diphenyl tetrazolium bromide (MTT) assay. One, 3, and 5 days after cell seeding, MTT solution (final concentration 1 mg/mL) was added, and cells were incubated for 1 h. The medium was then carefully removed and the dimethyl sulfoxide was added to each well. The amount of formazan crystals formed by viable cells was determined by measuring absorbance at 540 nm with a spectrophotometer (GE Healthcare, Piscataway, NJ, USA).

5. Single cell colony formation assay

Breast cancer cells were trypsinized to generate single cell suspensions and seeded at a low density (500 cells/well in 96-well plates) in Dulbecco's Modified Eagle's Medium-F12 supplemented with B-27 (Invitrogen) , 20 ng/mL epidermal growth factor (BD Biosciences), 10 ng/mL leukemia inhibitory factor (Invitrogen), and 20 ng/mL basic fibroblast growth factor (BD Biosciences). Seven to 14 days later, average numbers of colonies per well were calculated. These experiments were performed in triplicate.

6. Migration and invasion assays

To assess cell migratory ability, 5×10^4 cells were suspended in 100 μL of medium containing no FBS and were deposited in the upper chambers of a trans-well plate with 8.0-μm pores (BD Biosciences) and non-coated membranes. For the invasion assays, 5×10^4 cells were plated in 2% Matrigel™ (BD Biosciences) basement membrane matrix- or 5 μg/cm^2 type I rat tail collagen-coated upper chambers of trans-well plates with 8.0-μm pores. The lower chambers were filled with 600 μL of medium supplemented with 10% FBS, and the cells were incubated for between 24-48 h at 37□C depending on the cell line. Cells that migrated from the upper chambers to the bottom chambers were stained using a crystal violet solution (0.5% crystal

violet in 20% methanol) for 5 min. Unbound crystal violet was removed by rinsing with distilled water. The cells were then air dried, after which the crystal violet was eluted from the cells using a 1% sodium dodecyl sulfate (SDS) solution. The absorbance of the crystal violet was measured at 550 nm using a spectrophotometer (GE Healthcare).

7. Western blotting

Cells were lysed in RIPA buffer (Sigma, St. Louis, MO, USA), and proteins were separated using SDS-polyacrylamide gel electrophoresis and transferred to nitrocellulose membranes. The membranes were blocked using 5% skim milk in Tris-buffered saline containing 0.1% Tween-20 and incubated with primary antibodies directed against LOX, LOXL1, LOXL2, LOXL3 (Santa Cruz Biotechnology, Santa CruzCA, USA), LOXL4 (Abcam, Cambridge, MA, USA), Collagen I (Novus, Littleton, CO, USA), Collagen IV (Abcam), PLOD1, PLOD2, P4HA1, P4HA2 (Novus), or β-actin (Sigma) overnight at 4℃. The membranes were then incubated with horseradish peroxidase (HRP)-conjugated secondary antibodies (Santa Cruz Biotechnology). The blotted membranes were visualized using enhanced chemiluminescence reagents (GE Healthcare). Western blot quantification was performed using ImageJ software.

8. Animals and xenograft tumor models

All animal experiments were approved by the Seoul National University Hospital Biomedical Research Institute Animal Care and Use Committee (IACUC). 5- to 6-week-old female BALB/c nude mice were used. For the orthotopic xenograft tumor model, a total of 5×10^6 breast cancer cells per mouse were resuspended in Matrigel™ and injected into the 4th mammary glands of mice. The mice were separated into two groups of 5 mice each; group 1 received cells expressing non-silencing shRNA (control), while group 2 received cells expressing inducible LOXL4 shRNA (shLOXL4). No tumors grew in one of the 5 control group mice; only data from the remaining 4 control group mice were used. The lung metastatic tumor models were created by administering a total of 5×10^5 breast cancer cells per mouse (suspended in phosphate-buffered saline, PBS) into the tail veins of mice. The mice were separated into the same two groups described above; each group again had 5 mice. To induce LOXL4 knockdown in vivo, normal drinking water was replaced with 3% sucrose (added to increase palatability) with 2 mg/mL doxycycline (Sigma) and changed every 2-3 days. Primary tumor volume after implantation was measured using calipers. To determine xenograft tumor volumes, a modified ellipsoidal formula for volume (volume = 1/2[length x width2])

was used in which the length was the largest longitudinal diameter of the tumor and the width was the largest transverse diameter of the tumor.

9. Bioluminescent and RFP fluorescence imaging

To monitor primary tumor growth and metastasis non-invasively, bioluminescent imaging (BLI) was conducted on the IVIS 100 system (Caliper Life Sciences, Hopkinton, MA, USA). Once each week, the firefly luciferase substrate D-luciferin (Promega, San Luis Obispo, CA, USA) was injected intraperitoneally at a dose of 150 mg/kg, and images of the tumor and lung areas were acquired 10 minutes later to evaluate peak intensities. The sum of all detected photon counts within oval-shaped regions of interest (ROI, tumor or lung) was quantified in units of mean photons per second per square centimeter per steradian (p/s/cm2/sr) using Living Image® software (Caliper Life Sciences). For *ex vivo* RFP fluorescence imaging, mice were anesthetized and primary tumors and lung tissues were excised. *Ex vivo* RFP fluorescence images were obtained using the Maestro imaging system (CRi, Woburn, MA, USA); spectral fluorescence images consisting of autofluorescence spectra and spectra from RFP were then unmixed based on their spectral patterns using Maestro software (CRi).

10. Histological analysis

Histological analyses of primary tumors and cancer nodules in the lungs were performed. The primary tumors and lungs were removed 6 or 10 weeks after control or shLOXL4 cells were injected. Hematoxylin and eosin (H&E), Masson's trichrome, or Picrosirius red stainings, and immunostaining using primary LOXL1 (Santa Cruz Biotechnology), LOXL4 (Abcam), Collagen I (Novus), Collagen IV (Abcam), PLOD1, PLOD2, P4HA1, and P4HA2 (Novus) antibodies and HRP-conjugated secondary antibodies (Santa Cruz Biotechnology) were performed. Histological images of the stained tissues were acquired using a microscope (Leica, Buffalo Grove, IL, USA) equipped with a CCD camera.

11. Multiphoton second harmonic generation microscopy and image analysis

Collagen second harmonic generation (SHG) images were collected using a two-photon Zeiss LSM 7 MP microscope (Carl Zeiss, Maple Grove, MN, USA) with a 20 × lens to assess the degree of collagen matrix remodeling. A Ti:sapphire laser (Chameleon, Coherent) was used. The excitation wavelength was 930 nm. The collagen SHG signal from the H&E-stained slides was collected using a 420-480 nm narrow bandpass emission filter. The same laser power and detector gain settings were used when acquiring all images. Three independent

experiments were conducted for samples from primary tumors of both the non-silencing shRNA (control) group and the inducible LOXL4 shRNA (shLOXL4) group. Different regions were analyzed for each independent experiment. A MATLAB (MathWorks, Natick, MA, USA) script was written to fit image cross-sections with a spatial correlation function. The Curvelet Transform denoising FIbeR Extraction algorithm (CT-FIRE, LOCI, University of Wisconsin, Madison, WI, USA), an open-source collagen analysis program, was used to automatically analyze individual fiber metrics such as length, width, and straightness, in the images.

12. Analysis of the BreastMark dataset

A public online tool, BreastMark, was used to examine the prognostic value of the putative genes in breast cancer patients. This database integrates gene expression and survival data from 26 datasets generated with 12 different microarray platforms and corresponds to approximately 17,000 genes in up to 4,738 samples. Overall survival (OS) was analyzed, and the median was used to dichotomize the data [59]. Median survival was evaluated in high and low LOXL4, collagen I, and collagen IV expression groups; the high expression group included the 25% of samples with the highest expression, and the low expression group included the 25% of samples with the lowest expression. Survival curves were generated based on Kaplan-Meier

estimates; the log-rank p value with one degree of freedom was used to identify differences in survival, and hazard ratios (HR) with 95% confidence intervals were computed using Cox regression analysis. A hazard ratio of greater than one indicates that the marker was associated with poor prognosis, while a ratio of less than one means that it was associated with good prognosis.

13. Statistical analyses

Mean values ± standard deviations for all data were calculated for the results of at least three independent experiments and were statistically evaluated using analysis of variance (ANOVA) and paired t-tests. Mann-Whitney U test was used for statistical analysis of the in vivo BLI lung images because the shLOXL4 population had larger values than the control population. For all tests, p-values of less than 0.05 were considered significant.

RESULTS

LOXL2, LOXL3, and LOXL4 expression are higher in MDA-MB-231 cells than in other human breast cancer cells

We measured the expression of LOX and LOXL1-4 in a total of 10 human breast cancer cell (hBCC) lines that are classified as either luminal (MCF-7, BT-474), HER2 (MDA-MB-453, SK-BR3, HCC1954), or TN (BT-549, MDA-MB-157, MDA-MB-231, MDA-MB-468, HCC1937) subtype, as well as in normal breast epithelial cells (MCF-10A). As shown in Figure 2-1A and C, LOX and LOXL2 expression were abundant in all of the hBCCs and in the normal breast epithelial cells. LOXL1 was highly expressed in both the luminal subtype cells (MCF-7, BT-474) and in two of the three HER2 subtype cells (MDA-MB-453, SK-BR3), but was expressed at very low levels in HER2 subtype HCC1954 cells and in the TN subtype cells (BT-549, MDA-MB-157, MDA-MB-231, MDA-MB-468, HCC1937). In contrast, LOXL3 and LOXL4 expression was higher in the TN subtype cells (BT-549, MDA-MB-157, MDA-MB-231, HCC1937) than in the other subtypes. Furthermore, LOXL2, LOXL3, and LOXL4 expression were higher in MDA-MB-231 cells than in the other TN cells (BT-549, MDA-MB-157, MDA-MB-468, HCC1937). In addition, LOXL4 expression was higher in MDA-MB-231 cells than the expression of the other LOX family members that were elevated in

TN cells. We also examined type I procollagen (collagen I) and collagen IV expression in the various hBCC types. Collagen I expression was higher in BT-549 cells, and collagen IV expression was higher in MCF-10A and MDA-MB-157 cells, than in the other hBCCs (Figure 2-1B and D).

LOXL4 knockdown promotes migration

Fluorescence microscopy confirmed that the lentiviral vector facilitated doxycycline-dependent inducible RFP expression (Figure 2-2A), and flow cytometry revealed that the efficiency of lentivirus-mediated RFP gene transfer was over 97% (Figure 2-2B). Real-time RT-PCR revealed that lentiviral transduction of LOXL4 shRNA decreased LOXL4 mRNA levels (0.32 ± 0.05-fold) compared to the control (Figure 2C, $P = 0.002$). LOXL3 and LOXL4 are identical except for three amino acids; due to this similarity, LOXL3 mRNA levels also decreased 0.67 ± 0.08-fold in LOXL4-knockdown cells compared to the control (Figure 2C, $P = 0.038$). Interestingly, LOXL1 mRNA levels increased 2.87 ± 0.09-fold in LOXL4-knockdown cells compared to the control (Figure 2-2C, $P = 0.0002$). Consistent with the real-time RT-PCR results, Western blot analysis revealed that LOXL3 (0.61 ± 0.28-fold, $P = 0.015$) and LOXL4 (0.51 ± 0.27-fold, $P < 0.001$)

protein levels were significantly decreased in LOXL4-knockdown cells compared to the control cells (Figure 2-2D). However, despite the increase observed in LOXL1 mRNA levels, LOXL4 knockdown did not change LOXL1 protein levels (Figure 2-2D). After the LOXL1 precursor protein is synthesized, it undergoes post-translational processing by bone morphogenetic protein 1 [60, 61]; this may explain the inconsistency observed in LOXL4-knockdown-induced changes in LOXL1 mRNA and protein levels.

The growth rates and colony forming capacity observed in LOXL4-knockdown MDA-MB-231 cells were similar to those of control MDA-MB-231 cells (Figure 2-2E and F). The migratory ability of LOXL4-knockdown cells increased 1.82 ± 0.24-fold in the trans-well migration assay (Figure 2-2G, $P < 0.001$). The invasive ability of LOXL4-knockdown cells also increased by 1.80 ± 0.46-fold in the Matrigel™ matrix-coated trans-well assay (Figure 2-2H, $P = 0.0001$) and 1.78 ± 0.23-fold in the type I rat tail collagen-coated trans-well assay (Figure 2-2I, $P < 0.001$) compared to control cells. Cell characterization assays after LOXL4 knockdown were also conducted using MCF-7 (luminal subtype) and BT-549 (TN subtype) breast cancercells. LOXL4-knockdown and control MCF-7 cells had similar growth rates (Figure 2-3C), but growth rates decreased in

LOXL4-knockdown BT-549 on days 3 and 5 after cell seeding compared to control BT-549 cells ($P < 0.001$, Figure 2-4C). The colony forming capacities of LOXL4-knockdown MCF-7 and BT-549 cells were similar to those of the respective control cells (Figure 2-3D and 2-4D). Migratory capacity did not differ between LOXL4-knockdown and control MCF-7 cells (Figure 2-3E-G), but migratory and invasive abilities increased in LOXL4-knockdown BT-549 in the trans-well migration (1.31 ± 0.07-fold, $P = 0.002$) and the Matrigel™ matrix (1.87 ± 0.34-fold, $P = 0.001$), and collagen (1.85 ± 0.20-fold, $P < 0.001$) trans-well invasion assays compared to control BT-549 cells (Figure 2-4E-G).

LOXL4 knockdown promotes primary tumor growth and lung metastatic tumor formation

We next investigated whether LOXL4 knockdown increased primary tumor growth and metastatic tumor formation in vivo. In an orthotopic xenograft model ($n = 4$ and 5 for the control and LOXL4-knockdown groups, respectively), LOXL4 knockdown increased tumor volumes in the 5th and 6th weeks after cancer cell injection compared to the control (Figure 2-5A, $P = 0.008$ and $P = 0.040$, 5th and 6th weeks, respectively). Bioluminescence images (BLI) and associated total flux values ($p/s/cm^2/sr$) were obtained using the IVIS system just before

mice were sacrificed. As expected, in vivo BLI signals were stronger in LOXL4-knockdown tumor sites ($6.13x10^7$ p/s/cm^2/sr) than in control tumor sites ($468.54x10^7$ p/s/cm^2/sr) (Figure 2-5B-C, P = 0.035). The gross appearance and ex vivo RFP fluorescence images showed bigger primary tumors from in LOXL4-knockdown mice than those from the control mice (Figure 2-5D). In the lung metastasis model, BLI signals indicated that the lung nodule formation ability of LOXL4-knockdown cells ($15.05x10^5$ p/s/cm^2/sr) was increased compared with that of control cells ($108.77x10^5$ p/s/cm^2/sr) (P = 0.014, Figure 2-5E-F). Images of the gross appearance of the lungs and of RFP fluorescence detection also clearly confirmed that LOXL4-knockdown increased numbers of lung tumor nodules compared to the control (Figure 2-5G).

LOXL4 knockdown increases collagen I and IV, PLOD1, PLOD2, P4HA1, and P4HA2 expression in xenograft tumor tissues

To investigate whether LOXL4 knockdown altered the structure of the ECM in tumor tissues, Picrosirius red and Masson's trichrome staining were conducted. Strongly stained regions were observed within both primary tumors and lung nodules (Figure 2-6A-B). Histological analysis of primary tumors confirmed that LOXL4 expression was downregulated in LOXL4-knockdown tumors (Figure 2-6C). Type I

procollagen (Collagen I) and IV immunohistochemical (IHC) staining intensities were stronger in LOXL4 knockdown tumors than in control tumors (Figure 2-6D). LOXL4 knockdown also increased PLOD1-2 and P4HA1-2 levels compared to controls (Figure 2-6E). Consistent with the IHC results, western blots revealed a trend towards decreased LOXL4 protein expression in LOXL4-knockdown tumors, although this difference was not statistically significant (Figure 2-6F-G). Type I procollagen (collagen I) and IV expression levels increased 3.30 ± 1.40-fold ($P = 0.01$) and 4.19 ± 0.46-fold ($P = 0.047$), respectively, in LOXL4-knockdown tumors (Figure 4F-G). PLOD1 (2.31 ± 1.13-fold, $P = 0.002$), PLOD2 (3.21 ± 0.10-fold, $P < 0.001$), and P4HA2 (2.74 ± 0.29-fold, $P = 0.048$) expression also increased in LOXL4-knockdown tumors compared to control tumors (Figure 2-6H-I). In addition, PLOD1 (1.29 ± 0.06-fold, $P = 0.047$) and PLOD2 (1.49 ± 0.18-fold, $P = 0.013$) expression also increased in LOXL4-knockdown MDA-MB-231 cells relative to control cells (Figure 2-7). IHC staining of collagen I and IV, PLOD1-2, and P4HA1-2 in lung metastatic tissues revealed that LOXL4 expression was suppressed in LOXL4-knockdown lung tumors (Figure 2-6J). Collagen I and IV staining was stronger in LOXL4-knockdown lung tumors than in

control tumors (Figure 2-6K); PLOD1 and P4HA1-2 staining were also strong in LOXL4-knockdown lung tumors (Figure 2-6L-M).

LOXL4 knockdown promotes thickening of collagen fibers

We then used SHG imaging to examine whether LOXL4 knockdown altered collagen fiber structure and organization. Collagen fiber quantification was conducted using CT-FIRE, an open-source software package that was developed to automatically quantify individual collagen fibers in SHG images (http://loci.wisc.edu/software/ctfire) [62]. Fiber lengths and widths were calculated as pixel values. Straightness was calculated by dividing the distance between each fiber's end points by the fiber path; the scale for this metric was 0-1, with 1 indicating a straight line. Although collagen fiber length and straightness did not differ between control and LOXL4-knockdown tissues, collagen fiber width was elevated in LOXL4-knockdown tumors compared to control tumors (Figure 2-8A-B, P = 0.041).

Low LOXL4 and high collagen expression are associated with poor overall survival

The BreastMark website was used to explore the association between LOXL4 and collagen I and IV expression and OS in breast cancer patients. A total of 584 samples from 11 datasets were analyzed,

including 169 events from BreastMark, and the samples were separated into high and low LOXL4 expression groups. Kaplan–Meier plots revealed that OS was significantly shorter in the low LOXL4 level group (Figure 2–9A, P = 0.004, HR = 0.6395). Interestingly, OS was poorest in breast cancer patients with both low LOXL4 levels and high collagen I or IV expression (Figure 2–9B–C, P = 0.037, HR = 0.6718 and P = 0.037, HR = 0.6619, respectively). We also analyzed OS in a set of 101 patients that included 36 who were diagnosed with TNBC using the PAM50 assay. Low LOXL4 expression was also associated with poor OS in these patients (Figure 2–9D, P = 0.009, HR = 0.427). While the trend towards an association between the combination of low LOXL4 and high collagen I expression and poorer OS did not reach significance (Figure 2–9E, P = 0.061, HR=0.4621), the low LOXL4 and high collagen IV expression combination was significantly associated with poorer OS in TNBC patients (Figure 2–9F, P = 0.008, HR = 0.3006).

DISCUSSION

In the present study, we demonstrated that knockdown of LOXL4 expression promoted primary tumor growth and lung metastasis in MDA-MB-231 cell xenograft models of breast cancer. These increases in tumor growth and metastasis were accompanied by alterations in the synthesis, deposition, structure of collagen, and specifically by an increase in bundle thickness. Furthermore, we found that low LOXL4 expression was associated with poorer overall survival in breast cancer patients. To the best of our knowledge, this is the first report to demonstrate a link between low LOXL4 expression and increased progression in TNBC.

First, we evaluated the expression of the LOX family members, as well as collagen I and IV, in a diverse set of breast cancer cell lines. LOXL4 expression was higher in MDA-MB-231 cells, which are aggressive TNBC cells, than in cells belonging to the luminal and HER2 subtypes. We then examined the effects of shRNA-mediated LOXL4 knockdown in MDA-MB-231 cells; knockdown of LOXL4 increased the migratory and invasive abilities of these cells. While Kirschmann *et al.* reported that LOX and LOXL2 expression were most strongly associated with invasive potential in both highly invasive and metastatic breast cancer cell lines [63], our results indicate that LOXL4 also suppresses invasion and migration in MDA-MB-231 cells. These

findings are inconsistent with a previous report that high LOXL4 mRNA levels may promote the transition from the solid to the effusion state in breast carcinomas [64]. We also found that LOXL4 expression differed among the hBCCs based on the breast cancer subtype to which they belonged. It is therefore likely that the role of LOXL4 may depend on heterogenous traits that vary in different types of breast cancer. Additional studies are needed to investigate the different roles of LOXL4 in breast cancer subtypes, particularly in TNBC.

Although recent studies have examined the role of LOXL4 in breast cancer, the explanation for the seemingly contradictory results obtained in cell lines and in xenograft models remains unclear. In our orthotopic primary tumor and lung metastasis models, we showed that LOXL4 knockdown increased primary tumor growth and metastasis in MDA-MB-231 cells. The authors of the one other study using LOXL4-knockdown MDA-MB-231 cells concluded that LOXL4 knockdown did not affect primary MDA-MB-231 cell tumor growth, but decreased spontaneous metastasis of MDA-MB-231 cells to the lungs in SCID and non-obese diabetic-SCID mice. The recruitment of CD11b-positive bone marrow-derived cells to sites of metastasis in the lungs was thought to underlie this effect [55]. These results, which contradict the findings of the present study, may be due to the use of

different lung metastasis models, as well as differences in the tumor microenvironments of the host mice.

In this study, LOXL4 knockdown increased collagen I and IV accumulation in both primary and lung tumor tissues in the xenograft models. PLOD1-2 and P4HA1-2, enzymes that are critical for collagen synthesis, may be predictive biomarkers for human cancer progression and metastasis [44-46]. Intriguingly, we found that PLOD1-2 and P4HA1-2 expression were elevated in LOXL4-knockdown primary and lung tumors. The increases in collagen I and IV expression in LOXL4-knockdown tumors might be associated with this increase in PLOD1-2 and P4HA1-2 expression, which is likely regulated by LOXL4-mediated intracellular signaling. In addition, NADPH oxidase (NOX) family genes, which also have pro-fibrotic effects, regulate the ECM and collagen synthesis in response to other signaling mechanisms, such as TGF-β and reactive oxygen species [65]. Although we did not investigate the effects of interactions between LOXL4 and NOX on collagen production in this study, NOX might also contribute to the LOXL4 knockdown-induced increase in collagen synthesis in breast cancer cells.

Straightened and aligned collagen fiber bundles were correlated with poor disease-specific and disease-free survival in an evaluation of the relationship between tumor-associated collagen signature-3

(TACS-3) and long-term survival rates in breast cancer patients [66]. Here, we found that collagen bundles were thicker in LOXL4-knockdown tumors than in control tumors, but no changes in the linearization or the length of the collagen fibers were found. This indicates that increased collagen bundle thickness in LOXL4-knockdown tumors might have accelerated primary tumor growth and lung metastasis in the MDA-MB-231 xenograft model.

Although extensive preclinical research has advanced our understanding of the mechanisms by which the LOX family increases fibrosis in the ECM, few studies have linked LOXL4 expression with clinical outcomes in breast cancer patients. A recent study found that LOXL4 was downregulated in hepatocellular carcinoma, and this downregulation was closely correlated with worse clinical outcomes [67]. Similarly, based on an OS analysis using data from the public database at the BreastMark website, we found that low LOXL4 expression was also associated with poor OS in breast cancer patients, suggesting that LOXL4 expression could be a useful prognostic marker in breast cancer. Moreover, this relationship between low LOXL4 expression and poor clinical outcome was strongest in patients with TNBC. Finally, OS was worst in TNBC patients with both low LOXL4 and high collagen IV expression.

In this study, we demonstrated that low LOXL4 expression is associated with increases in the progression of aggressive TNBC. However, because LOXL4 expression is also associated with other risk factors, particularly collagen levels and structural changes in the ECM, future studies with larger patient populations are needed to determine whether low LOXL4 levels can serve as an independent prognostic factor in TNBC.

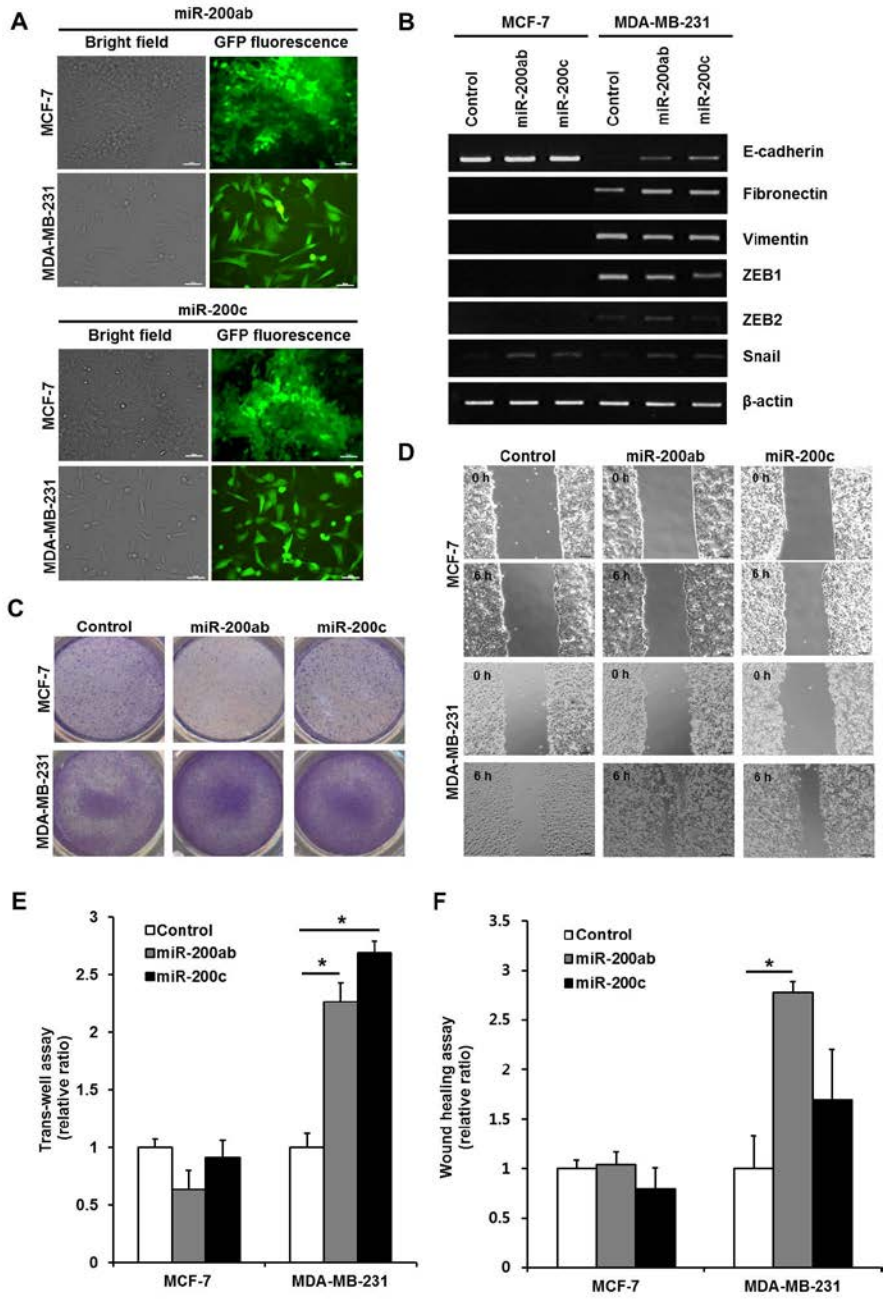

Figure 1-1. Comparison of gene expression and migration in miR-200b/200a/429 or miR-141/200c-transduced MCF-7 and MDA-MB-231 cells. (A) Fluorescence images of green fluorescent protein in MCF-7 and MDA-MB-231 cells that were transduced using lentivirus

encoding both GFP and miR-200 family members. Scale bar, 50 μm (B) RT-PCR analysis of genes related to epithelial-mesenchymal transition (E-cadherin, fibronectin, vimentin, ZEB1, ZEB2, and snail). (C) Images of the crystal violet-stained cells that migrated horizontally in the trans-well migration assay. (D) Images of the laterally migrated cells as determined using a wound-healing assay. (E) Quantitative analysis of the migratory ability of MCF-7 and MDA-MB-231 cells assessed using trans-well migration assay. (F) Quantitative analysis of the migratory ability of MCF-7 and MDA-MB-231 cells assessed using wound-healing assays. All experiments were performed at least in triplicate, and the values are the mean values ± standard deviation. *P < 0.05.

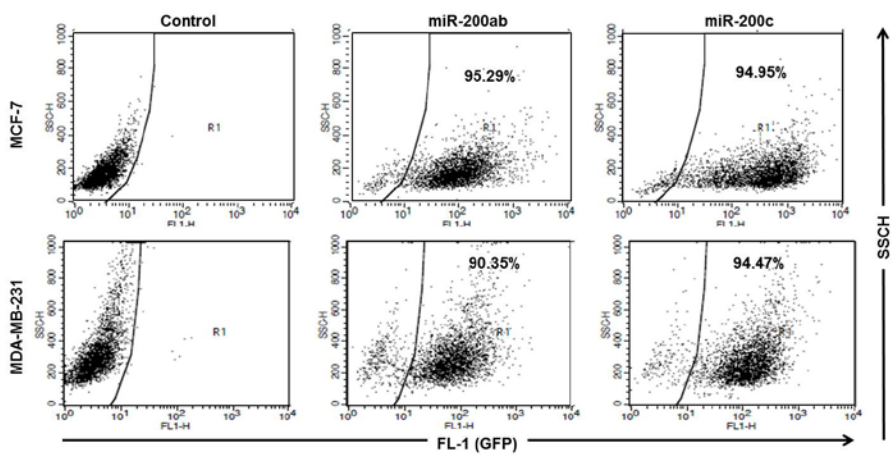

Figure 1-2. Flow cytometric analysis of GFP in miR-200b/200a/429 or miR-141/200c-transduced MCF-7 and MDA-MB-231 cells. Flow

cytometry analysis of the percentage of GFP-positive cells among the miR-200ab- and miR-200c-transduced MCF-7 and MDA-MB-231 cells.

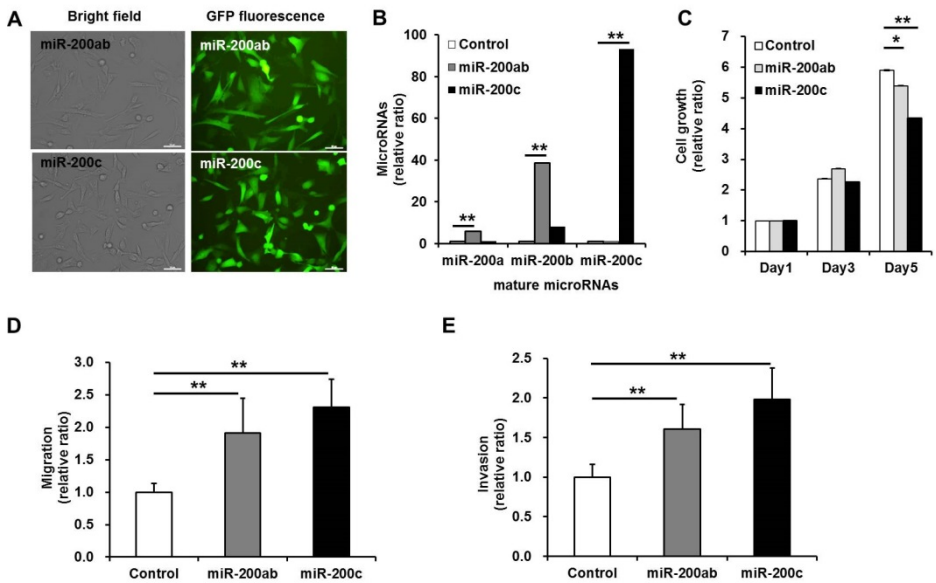

Figure 1-3. Proliferation, migration, and invasion of miR-200b/200a/429- or miR-141/200c-transduced MDA-MB-231 cells. (A) Fluorescence images of green fluorescent protein in MCF-7 and MDA-MB-231 cells that were transduced using lentivirus encoding both GFP and miR-200 family members. Scale bar; 50 μm (B) Quantitative real-time RT-PCR of microRNAs (miR-200a, miR-200b, and miR-200c). (C) MTT assay for analysis of cell proliferation. (D) Trans-well migration assay for the analysis of cell migration. (E) Trans-well invasion assay for the analysis of the invasive capacity. All

experiments were performed at least in triplicate, and the values are the mean values ± standard deviation. *P < 0.05, **P < 0.001.

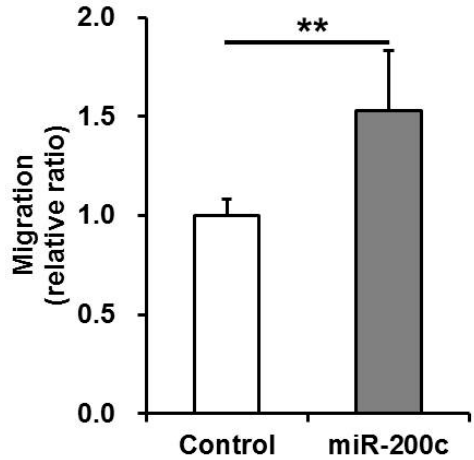

Figure 1-4. Migration in miR-141/200c-transduced MDA-MB-231 cells. Quantitative analysis of the migratory ability in of MDA-MB-231 and miR-141/200c-transduced MDA-MB-231 cells was performed in trans-well migration assay with 10% FBS in the lower chamber. All experiments were performed at least in triplicate, and the values are the mean values ± standard deviation. **P < 0.001.

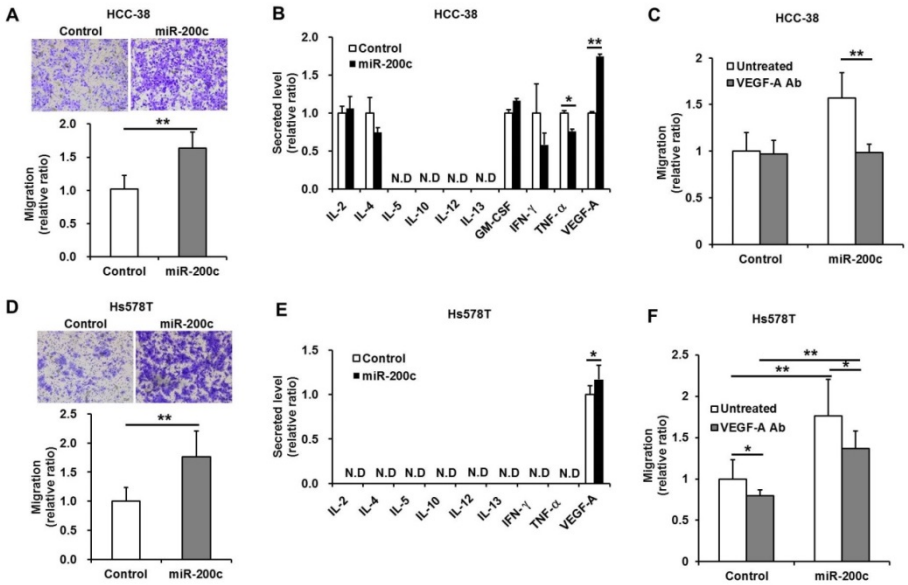

Figure 1-5. Migration in miR-141/200c-transduced HCC-38 and Hs578T cells treated with an anti-VEGF-A-neutralizing antibody. (A, D) Migration in miR-141/200c-transduced HCC-38 and Hs578T cells. Images of the crystal violet-stained cells that migrated horizontally in the trans-well migration assay (upper). The absorbance values of extracted crystal violet in migrated cells (lower). (B, E) Measurement of the secreted levels of cytokines and growth factors (IL-2, IL-4, IL-5, IL-10, IL-12, IL-13, GM-CSF, IFN-γ, TNF-α, and VEGF-A). (C, F) Trans-well migration of anti-VEGF-A-neutralizing antibody-treated cells. *P < 0.05, **P < 0.001.

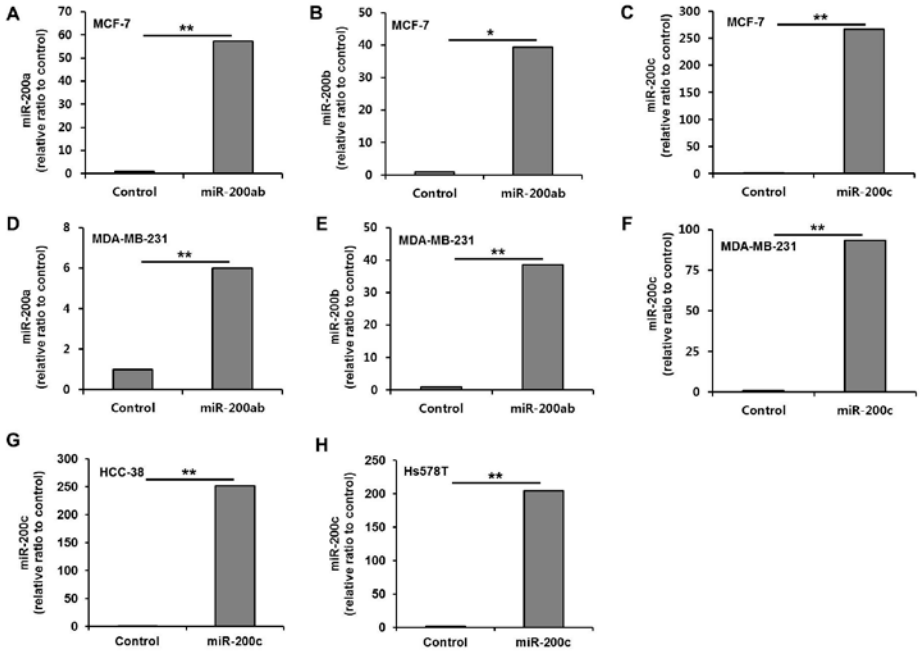

Figure 1-6. microRNA expression levels of miR-200 cluster transduced MCF-7, MDA-MB-231, HCC-38, and Hs578T cells. Quantitative real-time RT-PCR of microRNAs (miR-200a, miR-200b, and miR-200c). (A, B, C) microRNAs in MCF-7 cells. (D, E, F) microRNAs in MDA-MB-231. (G) microRNAs in HCC-38. (H) microRNAs in Hs578T. *P < 0.05, **P < 0.001.

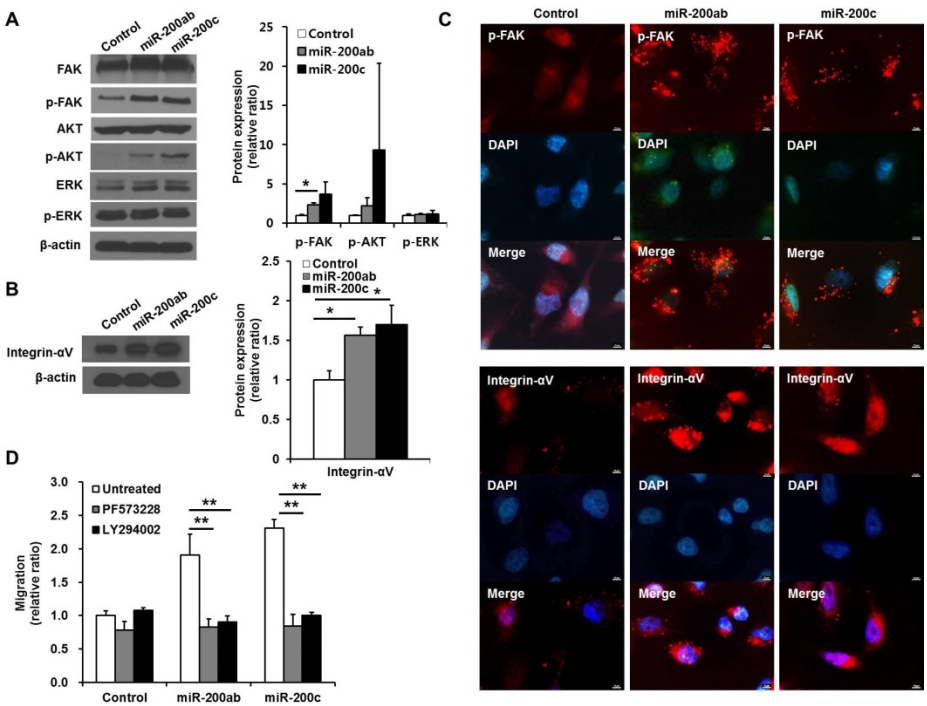

Figure 1-7. Signaling pathway associated with enhanced migration in miR-200b/200a/429 or miR-141/200c-transduced MDA-MB-231 cells. (A, B) Western blotting analysis of the levels of phosphorylated FAK, AKT, ERK, and integrin-αV expression. Densitometric quantifications of FAK, AKT, and ERK phosphorylation in the miR-200 family-transduced cells relative to control cells. β-actin was used as an internal reference. (C) Immunofluorescence analysis of phosphorylated FAK and integrin-αV. (D) Trans-well migration assay of FAK (PF573228) and PI3K/AKT (LY294002)-inhibitor-treated cells. All experiments were performed at least in triplicate, and the

values are the mean values ± standard deviation.. *P < 0.05, **P < 0.001, Scale bar, 10 μm.

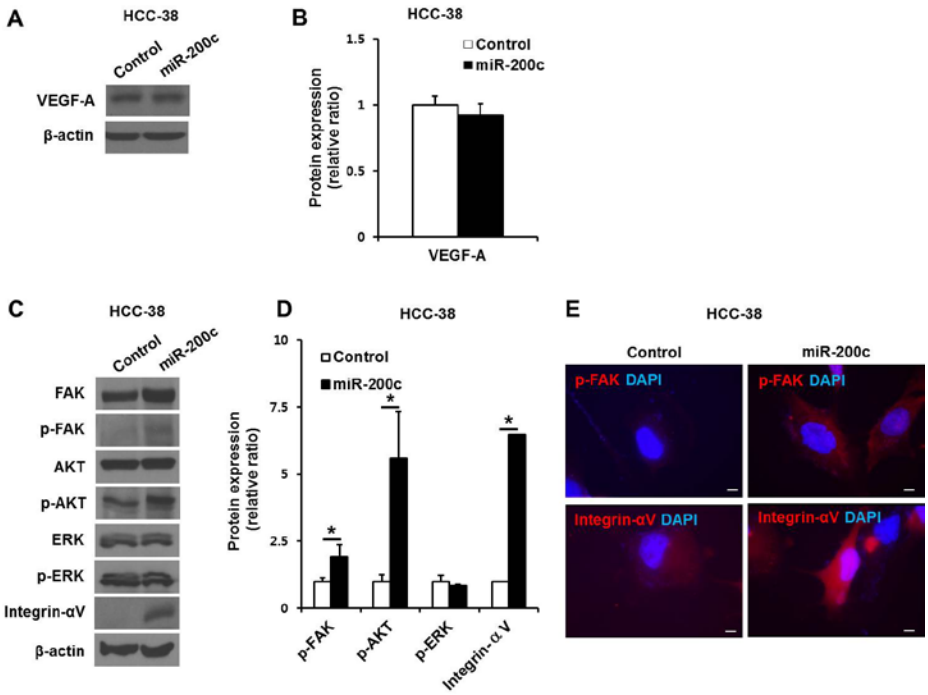

Figure 1-8. VEGF-A expression and signaling pathways associated with enhanced migration in miR-141/200c-transduced HCC-38 cells. (A) Representative image of western blotting analysis of VEGF-A levels. β-actin was used as an internal reference. (B) Densitometric quantification of VEGF-A in the miR-141/200c-transduced cells relative to the control cells. (C) Western blotting analysis of the levels of phosphorylated FAK, AKT, ERK, and integrin-αV expression. β-actin was used as an internal reference. (D) Densitometric quantification of FAK, AKT, and ERK phosphorylation in the miR-

141/200c-transduced cells relative to the control cells. (E) Immunofluorescence analysis of phosphorylated FAK and integrin-αV. *P < 0.05. Scale bar, 10 μm.

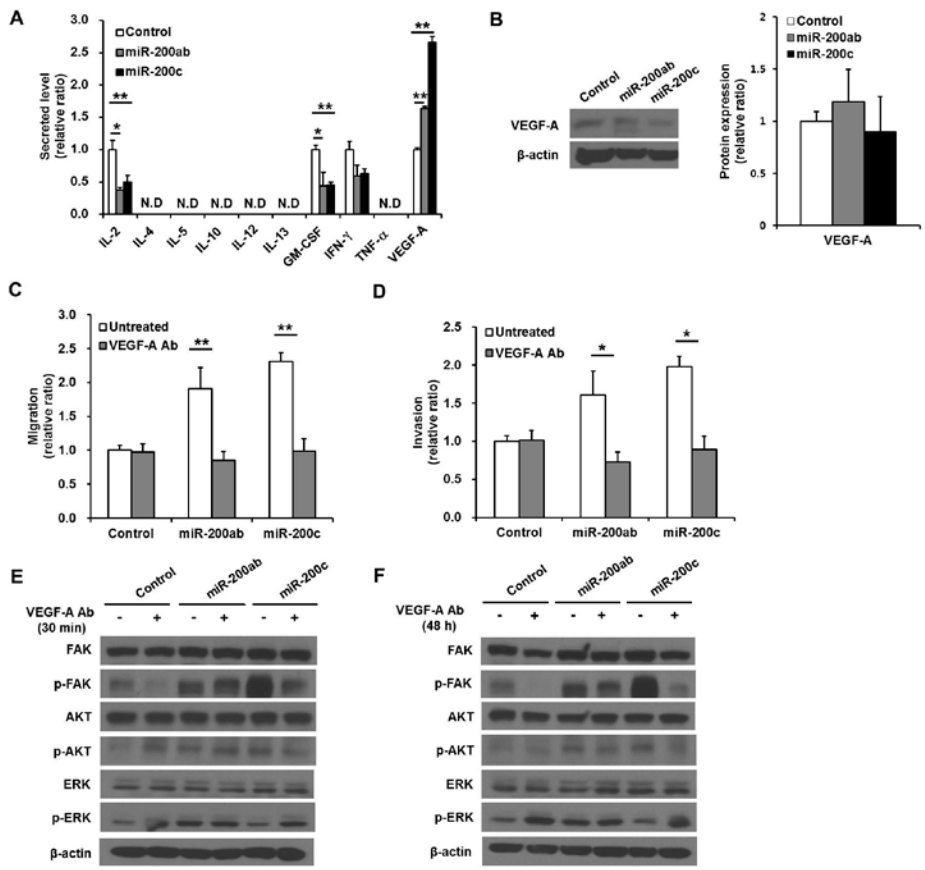

Figure 1-9. Migration and invasion in miR-200b/200a/429 or miR-141/200c-transduced MDA-MB-231 cells treated with an anti-VEGF-A-neutralizing antibody. (A) Measurement of the secreted levels of cytokines and growth factors (IL-2, IL-4, IL-5, IL-10, IL-12, IL-13, GM-CSF, IFN-γ, TNF-α, and VEGF-A). (B) Western blotting analysis of the levels of VEGF-A. (C) Trans-well migration

and (D) invasion assay of anti-VEGF-A-neutralizing antibody-treated cells. (E, F) Representative image of western blotting of phosphorylated AKT, FAK, and ERK and total AKT, FAK and ERK in cells treated with anti-VEGF-A-neutralizing antibodies for 30 min and 48 h. All experiments were performed at least in triplicate, and the values are the mean values ± standard deviation. N.D: not detectable. *P < 0.05, **P < 0.001.

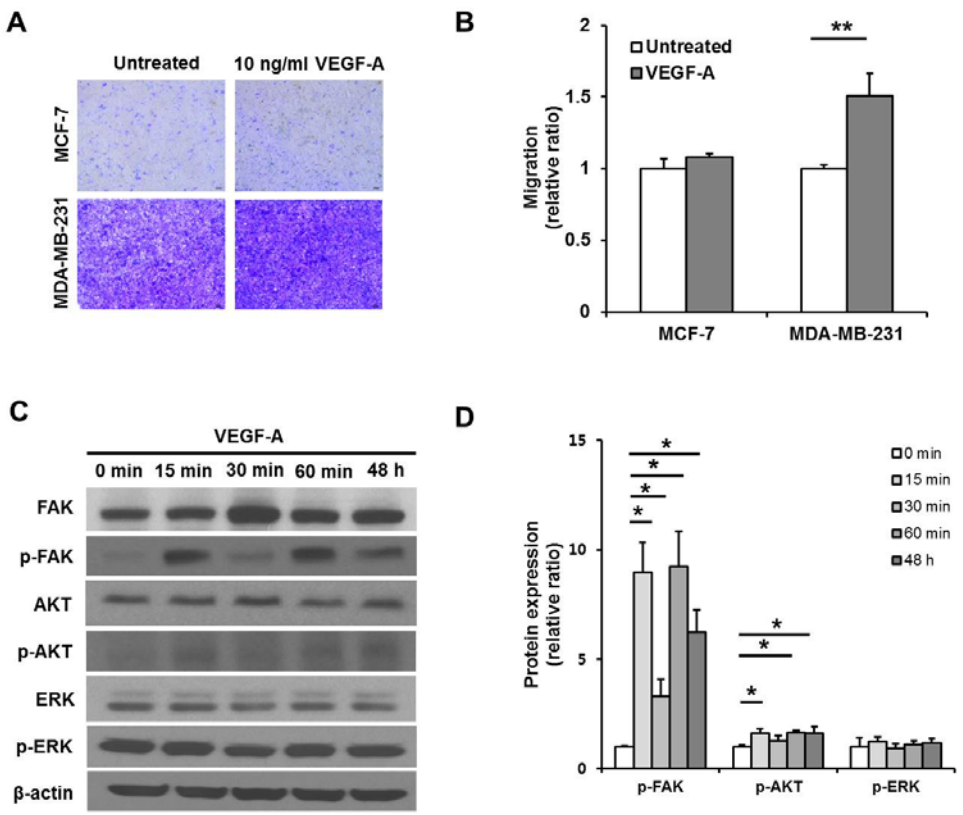

Figure 1-10. Migration and signaling pathways in VEGF-A-stimulated MDA-MB-231 cells. (A) Images of the crystal violet-stained cells that migrated horizontally in the trans-well migration assay. (B) The

absorbance values of extracted crystal violet in migrated cells. (C) Representative image of western blotting of phosphorylated AKT, FAK and ERK and total AKT, FAK and ERK in MDA−MB−231 cells treated with VEGF−A. (D) Densitometric quantifications of phosphorylation levels of FAK, AKT, and ERK in the VEGF−A−treated cells relative to the untreated cells. β−actin was used as an internal reference. All experiments were performed at least in triplicate, and the values are the mean values ± standard deviation. *P < 0.05, **P < 0.001.

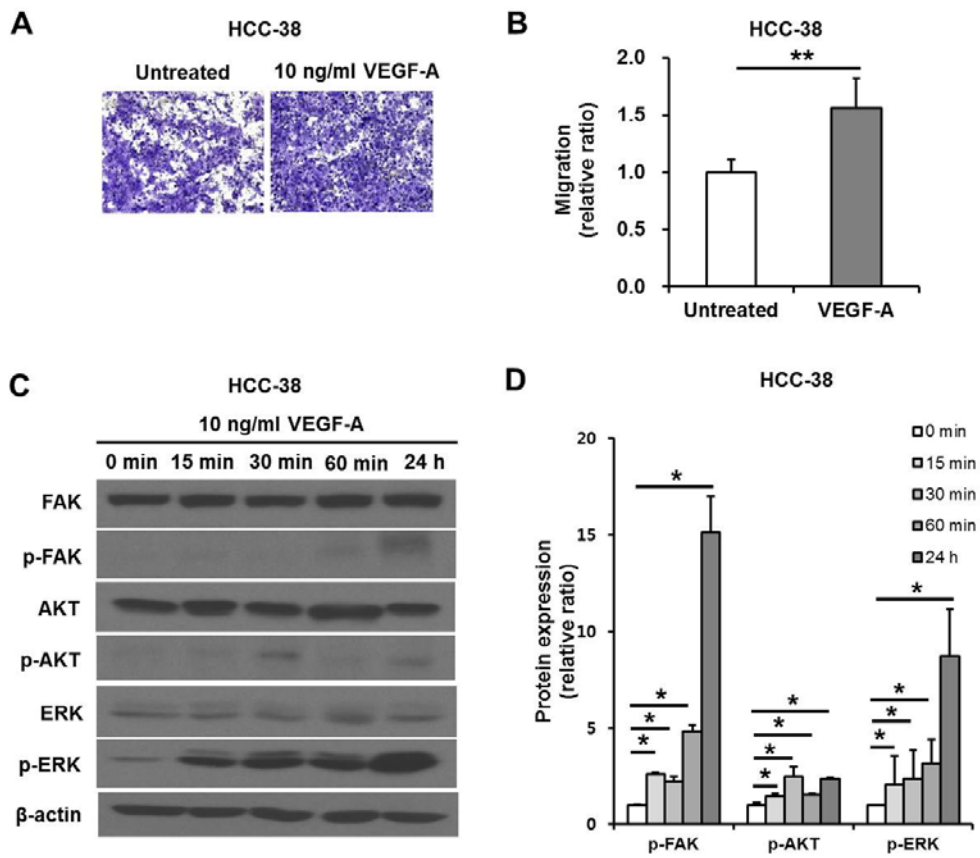

Figure 1-11. Migration and signaling pathways in VEGF-A-stimulated HCC-38 cells. (A) Migration in VEGF-A-stimulated HCC-38 cells. Images of the crystal violet-stained cells that migrated horizontally in the trans-well migration assay. (B) The absorbance values of extracted crystal violet in migrated cells (lower). (C) Representative image of western blotting of phosphorylated AKT, FAK and ERK and total AKT, FAK and ERK in HCC-38 cells treated with VEGF-A. (D) Densitometric quantification of VEGF-A in the miR-141/200c-transduced cells relative to the control cells. β-actin was used as an internal reference. *P < 0.05, **P < 0.001.

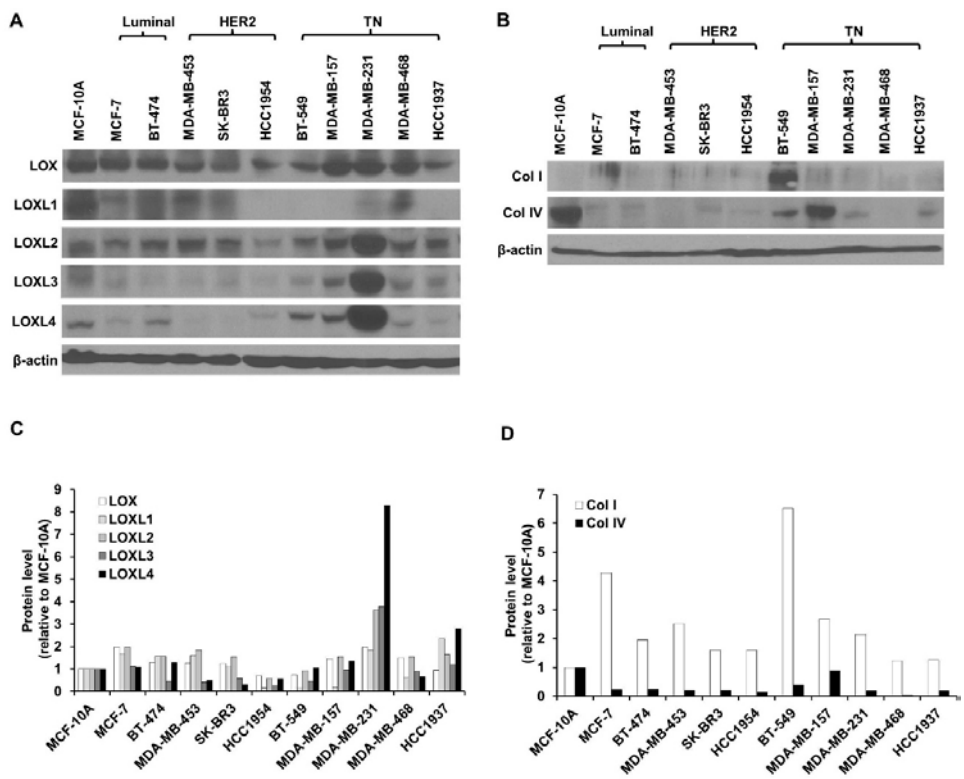

Figure 2-1. LOX family member, collagen I, and collagen IV expression in various breast cancer cells. (A and B) Western blotting analysis of LOX family (LOX and LOXL1-4), collagen I, and collagen IV protein expression in normal breast epithelial cells (MCF-10A) and luminal (MCF-7, BT-474), HER2 (MDA-MB-453, SK-BR3, and HCC1954), and TN (BT-549, MDA-MB-157, MDA-MB-231, MDA-MB-468, and HCC1937) breast cancer cell lines. (C and D) LOX family, type I procollagen (collagen I), and collagen IV protein expression in breast cancer cells relative to MCF-10A cells.

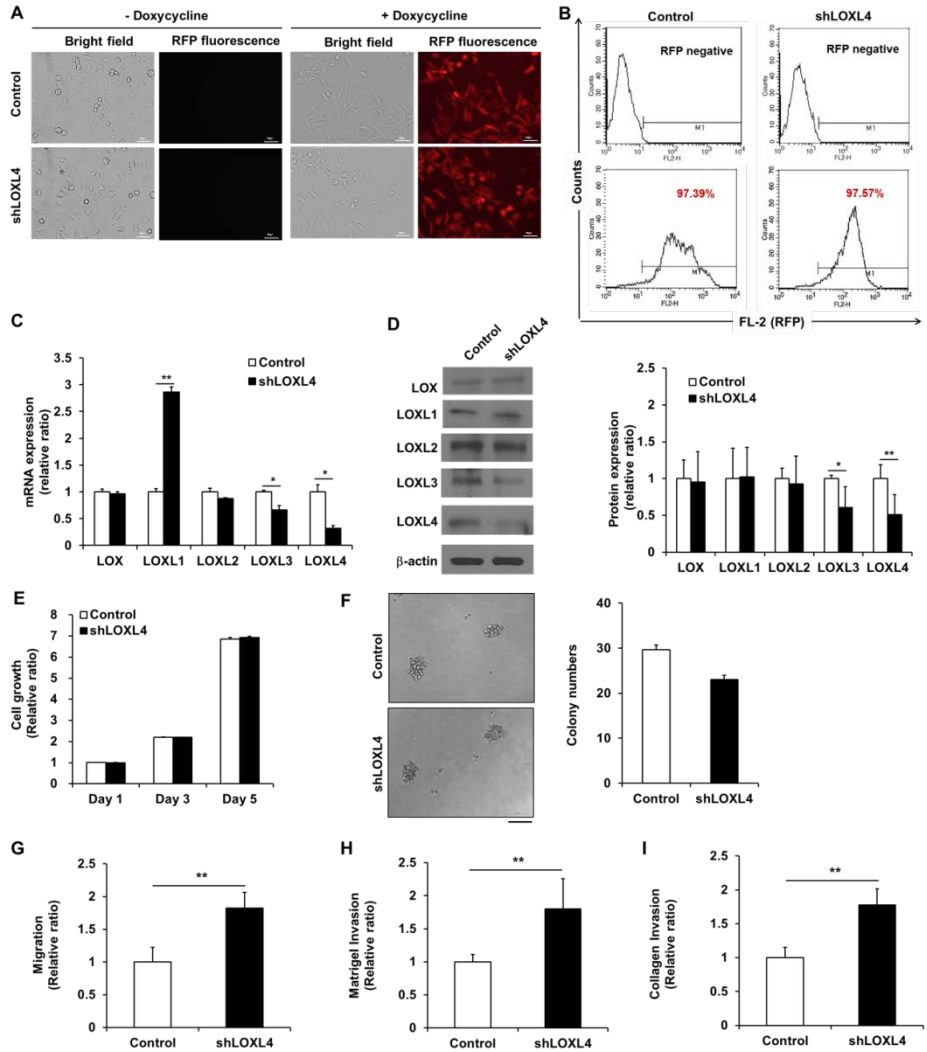

Figure 2-2. Establishment and characterization of the LOXL4 knockdown MDA-MB-231 cells. (A) Fluorescence images of doxycycline-inducible red fluorescent protein expression in MDA-MB-231 cells transduced with lentivirus encoding both RFP and either the non-silencing control vector or shLOXL4. Scale bar: 50 μm. (B) Flow cytometric analysis of the percentage of RFP-positive control or LOXL4-knockdown MDA-MB-231 cells. (C) Quantitative real-time

RT-PCR of LOX and LOXL1-4. (D) Western blotting analysis of LOX family member protein expression. (E) MTT assay for analysis of cell proliferation. (F) Single cell colony formation assay. Scale bar: 100 μm. (G) Trans-well migration assay for the analysis of cell migratory capacity. (H and I) Trans-well invasion assays for the analysis of cell invasion capacity. All experiments were performed at least in triplicate; means ± standard deviation of all experiments are shown. *P < 0.05. **P < 0.001. Scale bar: 50 μm.

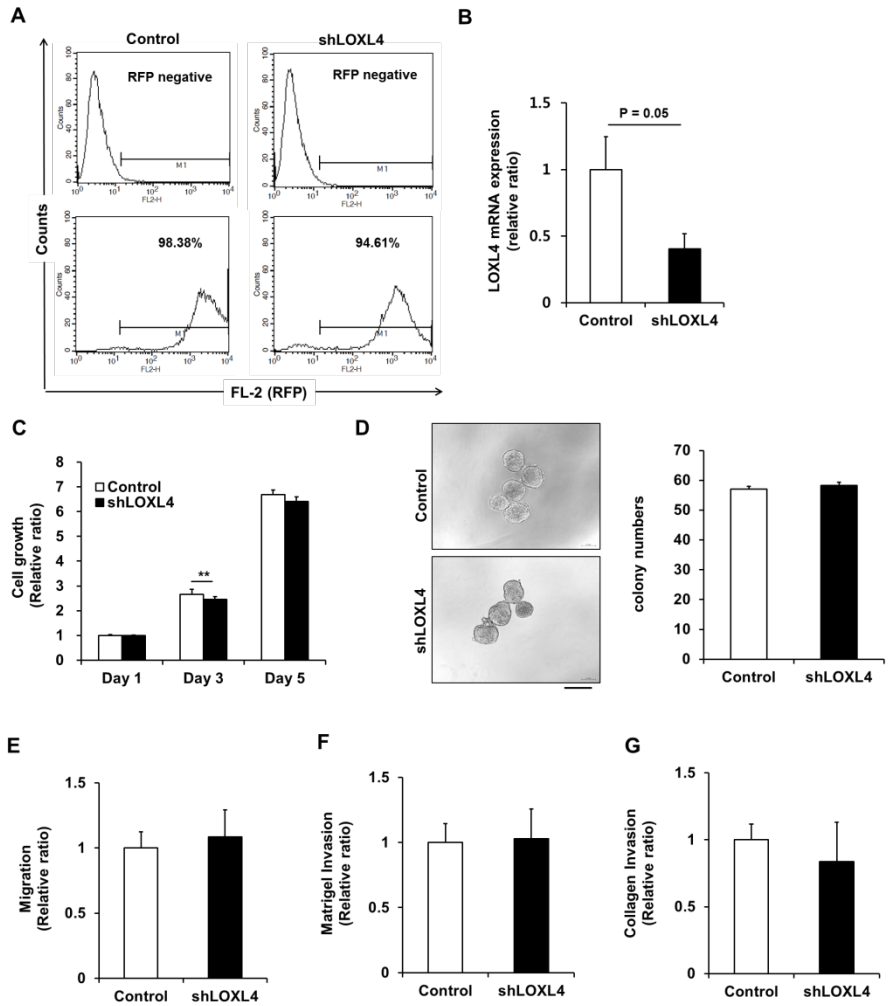

Figure 2-3. Establishment and characterization of LOXL4 knockdown MCF-7 cells. (A) Flow cytometric analysis of the percentage of RFP-positive control and LOXL4-knockdown MCF-7 cells. (B) Quantitative real-time RT-PCR of LOXL4. (C) MTT assay for analysis of cell proliferation. (D) Single cell colony formation assay. (E) Trans-well migration assay for the analysis of cell migratory capacity. (F and G) Trans-well invasion assays for the analysis of cell invasion capacity. All experiments were performed at least in triplicate; means ± standard

deviation of all experiments are shown. *P < 0.05. **P < 0.001. Scale bar: 200 μm.

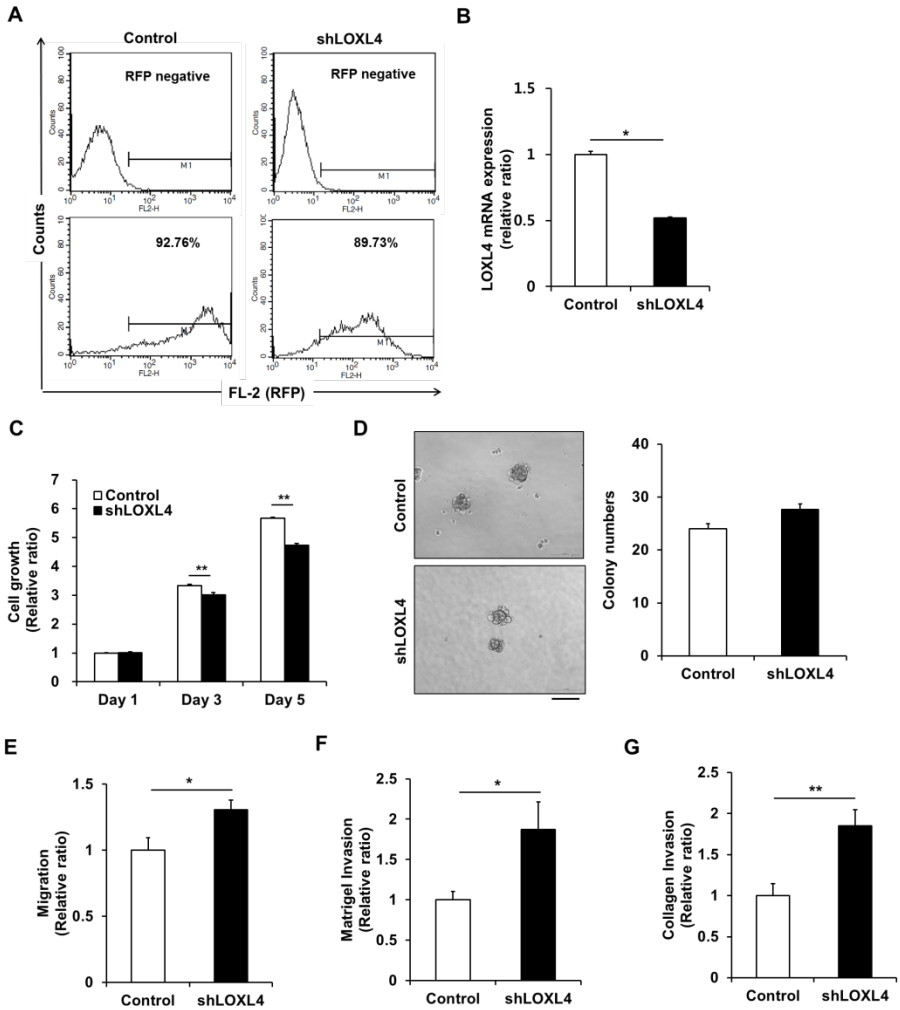

Figure 2-4. Establishment and characterization of LOXL4 knockdown BT-549 cells. (A) Flow cytometric analysis of the percentage of RFP-positive control and LOXL4-knockdown BT-549 cells. (B). Quantitative real-time RT-PCR of LOXL4. C. MTT assay for analysis of cell proliferation. (D) Single cell colony formation assay. (E)

Trans-well migration assay for the analysis of cell migratory capacity. (F and G) Trans-well invasion assays for the analysis of cell invasion capacity. All the experiments were performed at least in triplicate; means ± standard deviation of all experiments are shown. *P < 0.05. **P < 0.001. Scale bar: 100 μm.

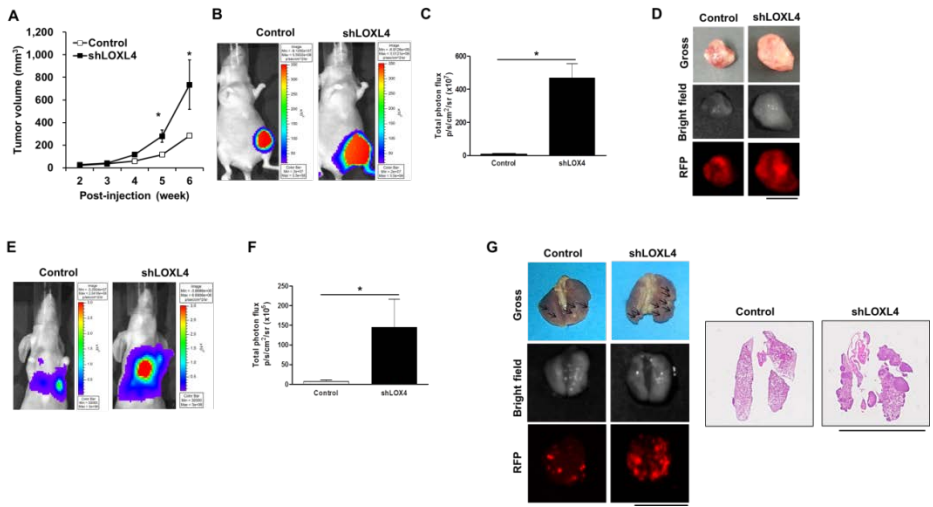

Figure 2-5. LOXL4 knockdown increased primary tumor growth and lung metastasis of MDA-MB-231 breast cancer cells. (A) Changes in tumor volume after injection of MDA-MB-231 cells transduced with control or shLOXL4. (B) Representative bioluminescence images of the tumors obtained with the IVIS system on day 41 after cancer cell injection. (C) Total flux values (p/s/cm2/sr) measured in bioluminescence images (day 41) of the primary tumors. Control and shLOXL4, n = 4 and 5, respectively. (D) Images of the final lung gross appearance and doxycycline-induced RFP in primary tumors. (E)

Representative bioluminescence images of tumor burdens in lungs obtained on day 56 after tail vein injections of cancer cells. n = 5. (F) Total flux (p/s/cm2/sr) measured in bioluminescence images of the metastatic lung burden (day 56). (G) Images of the final lung gross appearance, doxycycline-induced RFP in lung metastatic nodules, and H&E staining. Scale bar: 1 cm.

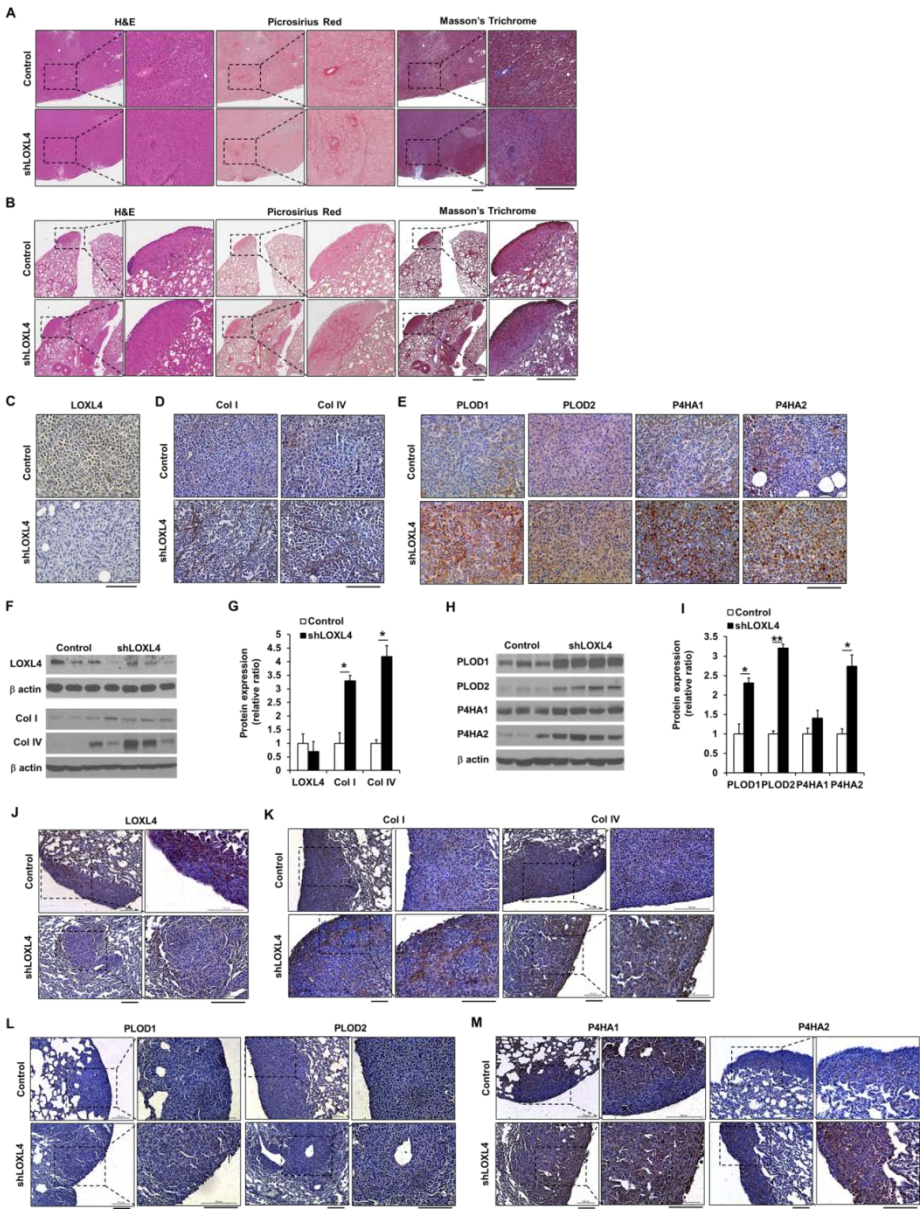

Figure 2-6. LOXL4 knockdown increases collagen synthesis and deposition. (A) Images of H&E-, Picrosirius red-, and Masson's trichrome-stained sections of primary tumors resulting from injection of control and LOXL4-knockdown cells. Scale bar: 400 μm. (B) Images of H&E-, Picrosirius red-, and Masson's trichrome-stained lung

sections after injection of control and LOXL4-knockdown cells. Scale bar: 400 μm. (C and D) Representative immunohistological (IHC) images of LOXL4, collagen I, and collagen IV staining in primary tumors. Scale bar: 100 μm. (E) Representative IHC images of PLOD1-2 and P4HA1-2 staining in primary tumors. Scale bar: 100 μm. (F) Representative images of Western blots for LOXL4, type I procollagen (collagen I), and collagen IV. (G) Densitometric quantification of LOXL4, type I procollagen (collagen I), and collagen IV expression in tumors. (H) Western blotting analysis of PLOD1-2 and P4HA1-2 expression in primary tumors. (I) Densitometric quantification of PLOD1-2 and P4HA1-2 expression in tumors. (J and K) Representative IHC images of LOXL4, collagen I, and collagen IV staining in the lungs. Scale bar: 100 μm. (L and M) Representative IHC images of PLOD1-2 and P4HA1-2 staining in the lungs. Scale bar: 200 μm. *$P < 0.05$. **$P < 0.001$.

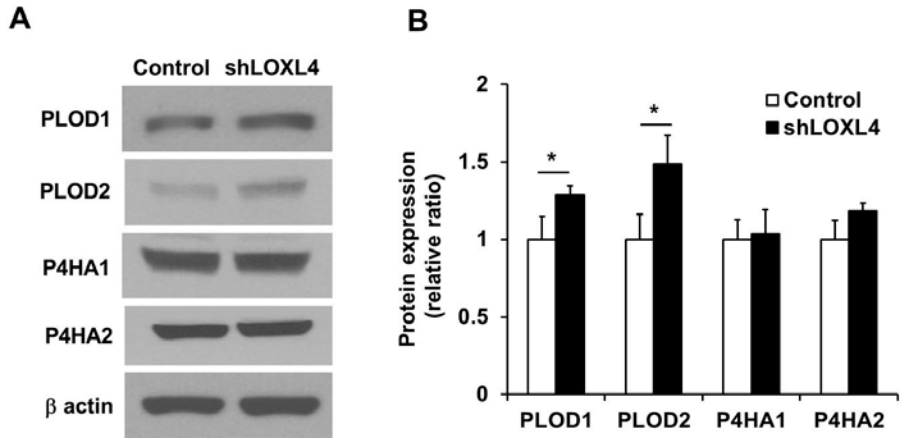

Figure 2-7. PLOD1, PLOD2, P4HA1, and P4HA2 expression in LOXL4 knockdown MDA-MB-231 cells. (A) Western blotting analysis of PLOD1-2 and P4HA1-2 protein expression. (B) Densitometric quantification of PLOD1-2 and P4HA1-2 expression.

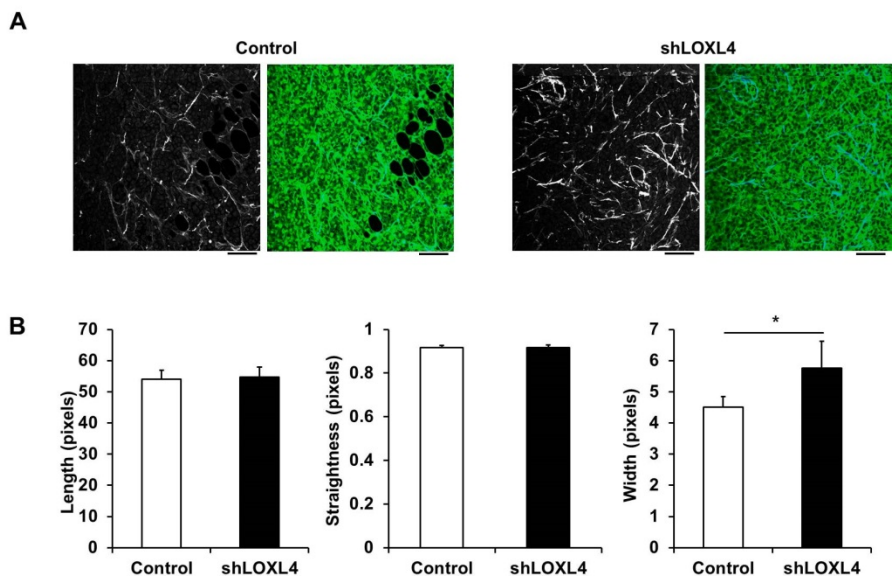

Figure 2-8. Second harmonic generation (SHG) imaging of control and LOXL4-knockdown primary tumor tissues. (A) Representative SHG images alone (left) and overlaid with the fluorescence images of

control and LOXL4-knockdown primary tumor tissues (right). (B) Quantification of collagen fiber lengths, straightness, and widths in control and LOXL4-knockdown primary tumor tissues. n = 5. *P < 0.05. Scale bar: 100 μm.

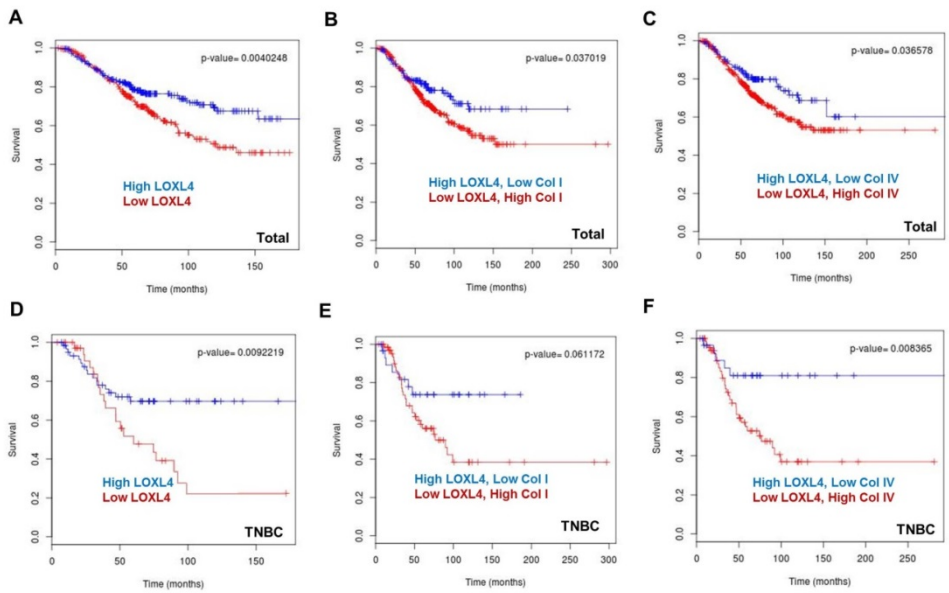

Figure 2-9. Kaplan-Meier plots of breast cancer patient survival based on LOXL4, collagen I, and collagen IV expression in the BreastMark dataset. (A) Low expression of LOXL4 was associated with a poor overall survival (OS) in total breast cancer. n = 584, number of events = 169, Hazard ratio (HR) = 0.6395 (0.4704-0.8694), score (log rank) test = 8.28, P = 0.004. (B) The combination of low LOXL4 and high collagen I expression was associated with poor OS in total breast cancer. n = 584, number of events = 169, HR = 0.6718 (0.4612-0.9787), score (log rank) test = 0.08, P = 0.037. (C) The combination

of low LOXL4 and high collagen IV expression was associated with a poor OS in total breast cancer. n = 584, number of events = 169, HR = 0.6619 (0.4483−0.9774), score (log rank) test = 15.36, P = 0.036. (D) Low expression of LOXL4 was associated with a poor OS in triple negative breast cancer (TNBC). n = 101, number of events = 36, HR = 0.427 (0.2207−0.8259), score (log rank) test = 6.78, P = 0.009. (E) The combination of low LOXL4 and high collagen I expression showed a borderline association with the OS in TNBC. n = 101, number of events = 36, HR=0.4621 (0.2018−1.058), score (log rank) test = 3.5, P = 0.061. (F) The combination of low LOXL4 and high collagen IV expression was associated with a poor OS in TNBC. n = 101, number of events = 36, HR = 0.3006 (0.1166−0.7749), score (log rank) test = 6.96, P = 0.008.

REFERENCES

1. Bartel, D.P. (2004). MicroRNAs: genomics, biogenesis, mechanism, and function. Cell *116*, 281-297.
2. Croce, C.M. (2009). Causes and consequences of microRNA dysregulation in cancer. Nature reviews. Genetics *10*, 704-714.
3. Lu, J., Getz, G., Miska, E.A., Alvarez-Saavedra, E., Lamb, J., Peck, D., Sweet-Cordero, A., Ebert, B.L., Mak, R.H., Ferrando, A.A., et al. (2005). MicroRNA expression profiles classify human cancers. Nature *435*, 834-838.
4. Korpal, M., Lee, E.S., Hu, G., and Kang, Y. (2008). The miR-200 family inhibits epithelial-mesenchymal transition and cancer cell migration by direct targeting of E-cadherin transcriptional repressors ZEB1 and ZEB2. The Journal of biological chemistry *283*, 14910-14914.
5. Gao, S.L., Wang, L.Z., Liu, H.Y., Liu, D.L., Xie, L.M., and Zhang, Z.W. (2014). miR-200a inhibits tumor proliferation by targeting AP-2gamma in neuroblastoma cells. Asian Pacific journal of cancer prevention : APJCP *15*, 4671-4676.
6. Korpal, M., Ell, B.J., Buffa, F.M., Ibrahim, T., Blanco, M.A., Celia-Terrassa, T., Mercatali, L., Khan, Z., Goodarzi, H., Hua, Y., et al. (2011). Direct targeting of Sec23a by miR-200s influences cancer cell secretome and promotes metastatic colonization. Nature medicine *17*, 1101-1108.
7. Dykxhoorn, D.M., Wu, Y., Xie, H., Yu, F., Lal, A., Petrocca, F., Martinvalet, D., Song, E., Lim, B., and Lieberman, J. (2009). miR-200 enhances mouse breast cancer cell colonization to form distant metastases. PloS one *4*, e7181.
8. Tuomarila, M., Luostari, K., Soini, Y., Kataja, V., Kosma, V.M., and Mannermaa, A. (2014). Overexpression of microRNA-200c predicts poor outcome in patients with PR-negative breast cancer. PloS one *9*, e109508.
9. Ceppi, P., Mudduluru, G., Kumarswamy, R., Rapa, I., Scagliotti, G.V., Papotti, M., and Allgayer, H. (2010). Loss of miR-200c expression induces an aggressive, invasive, and chemoresistant phenotype in non-small cell lung cancer. Molecular cancer research : MCR *8*, 1207-1216.
10. Korpal, M., and Kang, Y. (2008). The emerging role of miR-200 family of microRNAs in epithelial-mesenchymal transition and cancer metastasis. RNA biology *5*, 115-119.
11. Burk, U., Schubert, J., Wellner, U., Schmalhofer, O., Vincan, E., Spaderna, S., and Brabletz, T. (2008). A reciprocal repression between ZEB1 and members of the miR-200 family

promotes EMT and invasion in cancer cells. EMBO reports *9*, 582-589.

12. Carey, L.A., Dees, E.C., Sawyer, L., Gatti, L., Moore, D.T., Collichio, F., Ollila, D.W., Sartor, C.I., Graham, M.L., and Perou, C.M. (2007). The triple negative paradox: primary tumor chemosensitivity of breast cancer subtypes. Clinical cancer research : an official journal of the American Association for Cancer Research *13*, 2329-2334.
13. Cascione, L., Gasparini, P., Lovat, F., Carasi, S., Pulvirenti, A., Ferro, A., Alder, H., He, G., Vecchione, A., Croce, C.M., et al. (2013). Integrated microRNA and mRNA signatures associated with survival in triple negative breast cancer. PloS one *8*, e55910.
14. McArthur, K., Feng, B., Wu, Y., Chen, S., and Chakrabarti, S. (2011). MicroRNA-200b regulates vascular endothelial growth factor-mediated alterations in diabetic retinopathy. Diabetes *60*, 1314-1323.
15. Liu, G.T., Chen, H.T., Tsou, H.K., Tan, T.W., Fong, Y.C., Chen, P.C., Yang, W.H., Wang, S.W., Chen, J.C., and Tang, C.H. (2014). CCL5 promotes VEGF-dependent angiogenesis by down-regulating miR-200b through PI3K/Akt signaling pathway in human chondrosarcoma cells. Oncotarget *5*, 10718-10731.
16. Shi, L., Zhang, S., Wu, H., Zhang, L., Dai, X., Hu, J., Xue, J., Liu, T., Liang, Y., and Wu, G. (2013). MiR-200c increases the radiosensitivity of non-small-cell lung cancer cell line A549 by targeting VEGF-VEGFR2 pathway. PloS one *8*, e78344.
17. Vrba, L., Jensen, T.J., Garbe, J.C., Heimark, R.L., Cress, A.E., Dickinson, S., Stampfer, M.R., and Futscher, B.W. (2010). Role for DNA methylation in the regulation of miR-200c and miR-141 expression in normal and cancer cells. PloS one *5*, e8697.
18. Bracken, C.P., Gregory, P.A., Kolesnikoff, N., Bert, A.G., Wang, J., Shannon, M.F., and Goodall, G.J. (2008). A double-negative feedback loop between ZEB1-SIP1 and the microRNA-200 family regulates epithelial-mesenchymal transition. Cancer research *68*, 7846-7854.
19. Avery-Kiejda, K.A., Braye, S.G., Mathe, A., Forbes, J.F., and Scott, R.J. (2014). Decreased expression of key tumour suppressor microRNAs is associated with lymph node metastases in triple negative breast cancer. BMC cancer *14*, 51.
20. Lehmann, B.D., Bauer, J.A., Chen, X., Sanders, M.E., Chakravarthy, A.B., Shyr, Y., and Pietenpol, J.A. (2011). Identification of human triple-negative breast cancer subtypes and preclinical models for selection of targeted therapies. The Journal of clinical investigation *121*, 2750-2767.

21. Grigoriadis, A., Mackay, A., Noel, E., Wu, P.J., Natrajan, R., Frankum, J., Reis-Filho, J.S., and Tutt, A. (2012). Molecular characterisation of cell line models for triple-negative breast cancers. BMC genomics *13*, 619.
22. Engelman, J.A. (2009). Targeting PI3K signalling in cancer: opportunities, challenges and limitations. Nature reviews. Cancer *9*, 550-562.
23. Ihle, N.T., and Powis, G. (2009). Take your PIK: phosphatidylinositol 3-kinase inhibitors race through the clinic and toward cancer therapy. Molecular cancer therapeutics *8*, 1-9.
24. Zhao, X., and Guan, J.L. (2011). Focal adhesion kinase and its signaling pathways in cell migration and angiogenesis. Advanced drug delivery reviews *63*, 610-615.
25. Weiner, T.M., Liu, E.T., Craven, R.J., and Cance, W.G. (1993). Expression of focal adhesion kinase gene and invasive cancer. Lancet *342*, 1024-1025.
26. Romer, L.H., McLean, N., Turner, C.E., and Burridge, K. (1994). Tyrosine kinase activity, cytoskeletal organization, and motility in human vascular endothelial cells. Molecular biology of the cell *5*, 349-361.
27. Taliaferro-Smith, L., Oberlick, E., Liu, T., McGlothen, T., Alcaide, T., Tobin, R., Donnelly, S., Commander, R., Kline, E., Nagaraju, G.P., et al. (2015). FAK activation is required for IGF1R-mediated regulation of EMT, migration, and invasion in mesenchymal triple negative breast cancer cells. Oncotarget *6*, 4757-4772.
28. Keely, P.J. (2011). Mechanisms by which the extracellular matrix and integrin signaling act to regulate the switch between tumor suppression and tumor promotion. Journal of mammary gland biology and neoplasia *16*, 205-219.
29. Nicolini, A., Carpi, A., and Rossi, G. (2006). Cytokines in breast cancer. Cytokine Growth F R *17*, 325-337.
30. Pecot, C.V., Rupaimoole, R., Yang, D., Akbani, R., Ivan, C., Lu, C., Wu, S., Han, H.D., Shah, M.Y., Rodriguez-Aguayo, C., et al. (2013). Tumour angiogenesis regulation by the miR-200 family. Nature communications *4*, 2427.
31. Abid, M.R., Guo, S., Minami, T., Spokes, K.C., Ueki, K., Skurk, C., Walsh, K., and Aird, W.C. (2004). Vascular endothelial growth factor activates PI3K/Akt/forkhead signaling in endothelial cells. Arteriosclerosis, thrombosis, and vascular biology *24*, 294-300.
32. Hayakawa, K., Pham, L.D., Som, A.T., Lee, B.J., Guo, S., Lo, E.H., and Arai, K. (2011). Vascular endothelial growth factor regulates the migration of oligodendrocyte precursor cells. The

Journal of neuroscience : the official journal of the Society for Neuroscience *31*, 10666-10670.

33. Choi, Y.C., Yoon, S., Jeong, Y., Yoon, J., and Baek, K. (2011). Regulation of vascular endothelial growth factor signaling by miR-200b. Molecules and cells *32*, 77-82.
34. Lu, J., and Clark, A.G. (2012). Impact of microRNA regulation on variation in human gene expression. Genome research *22*, 1243-1254.
35. Mercurio, A.M., Lipscomb, E.A., and Bachelder, R.E. (2005). Non-angiogenic functions of VEGF in breast cancer. Journal of mammary gland biology and neoplasia *10*, 283-290.
36. Perrot-Applanat, M., and Di Benedetto, M. (2012). Autocrine functions of VEGF in breast tumor cells: adhesion, survival, migration and invasion. Cell adhesion & migration *6*, 547-553.
37. Butcher, D.T., Alliston, T., and Weaver, V.M. (2009). A tense situation: forcing tumour progression. Nature reviews. Cancer *9*, 108-122.
38. Kolacna, L., Bakesova, J., Varga, F., Kostakova, E., Planka, L., Necas, A., Lukas, D., Amler, E., and Pelouch, V. (2007). Biochemical and biophysical aspects of collagen nanostructure in the extracellular matrix. Physiological research / Academia Scientiarum Bohemoslovaca *56 Suppl 1*, S51-60.
39. Cox, T.R., and Erler, J.T. (2011). Remodeling and homeostasis of the extracellular matrix: implications for fibrotic diseases and cancer. Disease models & mechanisms *4*, 165-178.
40. Kalluri, R. (2003). Basement membranes: structure, assembly and role in tumour angiogenesis. Nature reviews. Cancer *3*, 422-433.
41. Provenzano, P.P., Eliceiri, K.W., Campbell, J.M., Inman, D.R., White, J.G., and Keely, P.J. (2006). Collagen reorganization at the tumor-stromal interface facilitates local invasion. BMC medicine *4*, 38.
42. Ohlund, D., Franklin, O., Lundberg, E., Lundin, C., and Sund, M. (2013). Type IV collagen stimulates pancreatic cancer cell proliferation, migration, and inhibits apoptosis through an autocrine loop. BMC cancer *13*, 154.
43. Kauppila, S., Stenback, F., Risteli, J., Jukkola, A., and Risteli, L. (1998). Aberrant type I and type III collagen gene expression in human breast cancer in vivo. The Journal of pathology *186*, 262-268.
44. Gilkes, D.M., Bajpai, S., Wong, C.C., Chaturvedi, P., Hubbi, M.E., Wirtz, D., and Semenza, G.L. (2013). Procollagen lysyl hydroxylase 2 is essential for hypoxia-induced breast cancer metastasis. Molecular cancer research : MCR *11*, 456-466.
45. Gilkes, D.M., Chaturvedi, P., Bajpai, S., Wong, C.C., Wei, H., Pitcairn, S., Hubbi, M.E., Wirtz, D., and Semenza, G.L. (2013).

Collagen prolyl hydroxylases are essential for breast cancer metastasis. Cancer research *73*, 3285-3296.

46. Xiong, G., Deng, L., Zhu, J., Rychahou, P.G., and Xu, R. (2014). Prolyl-4-hydroxylase alpha subunit 2 promotes breast cancer progression and metastasis by regulating collagen deposition. BMC cancer *14*, 1.
47. Maki, J.M., Tikkanen, H., and Kivirikko, K.I. (2001). Cloning and characterization of a fifth human lysyl oxidase isoenzyme: the third member of the lysyl oxidase-related subfamily with four scavenger receptor cysteine-rich domains. Matrix biology : journal of the International Society for Matrix Biology *20*, 493-496.
48. Kagan, H.M., and Li, W. (2003). Lysyl oxidase: properties, specificity, and biological roles inside and outside of the cell. J Cell Biochem *88*, 660-672.
49. Cox, T.R., Bird, D., Baker, A.M., Barker, H.E., Ho, M.W., Lang, G., and Erler, J.T. (2013). LOX-mediated collagen crosslinking is responsible for fibrosis-enhanced metastasis. Cancer research *73*, 1721-1732.
50. Erler, J.T., Bennewith, K.L., Nicolau, M., Dornhofer, N., Kong, C., Le, Q.T., Chi, J.T., Jeffrey, S.S., and Giaccia, A.J. (2006). Lysyl oxidase is essential for hypoxia-induced metastasis. Nature *440*, 1222-1226.
51. Palamakumbura, A.H., Jeay, S., Guo, Y., Pischon, N., Sommer, P., Sonenshein, G.E., and Trackman, P.C. (2004). The propeptide domain of lysyl oxidase induces phenotypic reversion of ras-transformed cells. The Journal of biological chemistry *279*, 40593-40600.
52. Wu, G., Guo, Z., Chang, X., Kim, M.S., Nagpal, J.K., Liu, J., Maki, J.M., Kivirikko, K.I., Ethier, S.P., Trink, B., et al. (2007). LOXL1 and LOXL4 are epigenetically silenced and can inhibit ras/extracellular signal-regulated kinase signaling pathway in human bladder cancer. Cancer research *67*, 4123-4129.
53. Weise, J.B., Rudolph, P., Heiser, A., Kruse, M.L., Hedderich, J., Cordes, C., Hoffmann, M., Brant, O., Ambrosch, P., Csiszar, K., et al. (2008). LOXL4 is a selectively expressed candidate diagnostic antigen in head and neck cancer. Eur J Cancer *44*, 1323-1331.
54. Kim, Y., Roh, S., Park, J.Y., Kim, Y., Cho, D.H., and Kim, J.C. (2009). Differential expression of the LOX family genes in human colorectal adenocarcinomas. Oncology reports *22*, 799-804.
55. Wong, C.C., Gilkes, D.M., Zhang, H., Chen, J., Wei, H., Chaturvedi, P., Fraley, S.I., Wong, C.M., Khoo, U.S., Ng, I.O., et al. (2011). Hypoxia-inducible factor 1 is a master regulator of breast cancer metastatic niche formation. Proceedings of the

National Academy of Sciences of the United States of America *108*, 16369-16374.

56. Erler, J.T., Bennewith, K.L., Cox, T.R., Lang, G., Bird, D., Koong, A., Le, Q.T., and Giaccia, A.J. (2009). Hypoxia-induced lysyl oxidase is a critical mediator of bone marrow cell recruitment to form the premetastatic niche. Cancer cell *15*, 35-44.
57. Ahn, S.G., Dong, S.M., Oshima, A., Kim, W.H., Lee, H.M., Lee, S.A., Kwon, S.H., Lee, J.H., Lee, J.M., Jeong, J., et al. (2013). LOXL2 expression is associated with invasiveness and negatively influences survival in breast cancer patients. Breast cancer research and treatment *141*, 89-99.
58. Wuest, M., Kuchar, M., Sharma, S.K., Richter, S., Hamann, I., Wang, M., Vos, L., Mackey, J.R., Wuest, F., and Loser, R. (2015). Targeting lysyl oxidase for molecular imaging in breast cancer. Breast Cancer Res *17*, 107.
59. Madden, S.F., Clarke, C., Gaule, P., Aherne, S.T., O'Donovan, N., Clynes, M., Crown, J., and Gallagher, W.M. (2013). BreastMark: an integrated approach to mining publicly available transcriptomic datasets relating to breast cancer outcome. Breast Cancer Res *15*, R52.
60. Barker, H.E., Cox, T.R., and Erler, J.T. (2012). The rationale for targeting the LOX family in cancer. Nature reviews. Cancer *12*, 540-552.
61. Uzel, M.I., Scott, I.C., Babakhanlou-Chase, H., Palamakumbura, A.H., Pappano, W.N., Hong, H.H., Greenspan, D.S., and Trackman, P.C. (2001). Multiple bone morphogenetic protein 1-related mammalian metalloproteinases process pro-lysyl oxidase at the correct physiological site and control lysyl oxidase activation in mouse embryo fibroblast cultures. The Journal of biological chemistry *276*, 22537-22543.
62. Bredfeldt, J.S., Liu, Y., Pehlke, C.A., Conklin, M.W., Szulczewski, J.M., Inman, D.R., Keely, P.J., Nowak, R.D., Mackie, T.R., and Eliceiri, K.W. (2014). Computational segmentation of collagen fibers from second-harmonic generation images of breast cancer. Journal of biomedical optics *19*, 16007.
63. Kirschmann, D.A., Seftor, E.A., Fong, S.F., Nieva, D.R., Sullivan, C.M., Edwards, E.M., Sommer, P., Csiszar, K., and Hendrix, M.J. (2002). A molecular role for lysyl oxidase in breast cancer invasion. Cancer research *62*, 4478-4483.
64. Sebban, S., Davidson, B., and Reich, R. (2009). Lysyl oxidase-like 4 is alternatively spliced in an anatomic site-specific manner in tumors involving the serosal cavities. Virchows Archiv : an international journal of pathology *454*, 71-79.

65. Dosoki, H., Stegemann, A., Taha, M., Schnittler, H., Luger, T.A., Schroder, K., Distler, J.H., Kerkhoff, C., and Bohm, M. (2016). Targeting of NADPH oxidase in vitro and in vivo suppresses fibroblast activation and experimental skin fibrosis. Experimental dermatology.
66. Conklin, M.W., Eickhoff, J.C., Riching, K.M., Pehlke, C.A., Eliceiri, K.W., Provenzano, P.P., Friedl, A., and Keely, P.J. (2011). Aligned collagen is a prognostic signature for survival in human breast carcinoma. The American journal of pathology *178*, 1221-1232.
67. Tian, M., Liu, W., Jin, L., Jiang, X., Yang, L., Ding, Z., Shen, Y., Peng, Y., Gao, D., Li, L., et al. (2015). LOXL4 is downregulated in hepatocellular carcinoma with a favorable prognosis. International journal of clinical and experimental pathology *8*, 3892-3900.

국문초록

서론: microRNA-200 (miR-200) family 는 E-Cadherin 의 전사억제인자인 ZEB1 과 ZEB2 의 발현을 억제하여 상피간엽이행 (Epithelial to Mesenchymal Transition)에 중요한 조절 인자로 알려져 있으나 유방암세포의 이동성과 침윤성 관련하여 miR-200 family 의 역할은 논란이 많다. 또한 lysyl oxidase-like 4 (LOXL4)는 lysyl oxidase (LOX) family 중 하나로 세포외 기질 변형과 세포의 증식 및 생존과 관련된 신호전달기전에 관여하는 것으로 알려져 있으나 유방암 진행과 전이에서 LOXL4 의 역할은 명확히 밝혀져 있지 않다. 따라서 본 연구에서는 miR-200 이 어떠한 기전에 의해 유방암 아형 중 예후가 가장 나쁜 삼중음성 유방암세포의 이동과 침윤 능력을 변화시키는지 규명하고자 한다. 또한 LOXL4 가 어떠한 기전에 의해 삼중음성 유방암 형성과 전이를 조절하는가를 규명하고 유방암 환자의 예후인자로서의 의의를 분석하고자 한다.

실험방법: 렌티바이러스 시스템을 이용해 miR-200b/200a/429 cluster 혹은 miR-141/200c cluster 와 녹색형광단백질 (GFP)을 안정적으로 발현하는 삼중음성 유방암세포인 MDA-MB-321 세포주와 LOXL4 short hairpin RNA (shLOXL4), 적색형광단백질 (RFP), 루시퍼라제 (firefly luciferase)와 녹색형광단백질을 발현하는 MDA-MB-321 세포주를 수립하였다. 유전자 발현은 실시간 중합효소연쇄반응

(real-time RT-PCR)이나 역전사 중합효소 연쇄반응 (RT-PCR)으로 분석하였다. 이동과 침윤 능력은 트랜스웰 (trans-well)이나 운드힐링 (wound-healing) 실험법으로 확인하였다. 세포에서 분비된 사이토카인과 성장 인자들은 바이오플랙스 200 멀티플랙스 (Bio-Plex 200 multiplex) 어레이 시스템으로 정량화하였다. 세포 내 신호 전달을 분석하기 위해 웨스턴 분석과 면역형광염색을 수행했다. 6 주령 면역결핍마우스 (BALB/c nude)의 유방의 지방패드나 꼬리 정맥에 유방암 세포를 주입하여 일차암과 폐전이 종양동물모델을 만들었다. 일차암 부피는 디지털캘리퍼스로 측정하였고 생체발광영상장비 (IVIS)와 생체광학장비 (Maestro)를 이용하여 일차암과 폐전이암을 분석하였다. 적출한 종양조직에서 H&E 염색, 특수염색 (Picrosirius red, Masson's trichrome)과 면역염색을 수행하였다. 콜라겐 섬유의 길이, 평면성과 두께를 정량화 하기 위해 제 2 고조파 발생 영상 기법 (Second-harmonic generation imaging, SHG)을 사용하였다. 퍼블릭 데이터베이스 (BreastMark)를 사용하여 LOXL4, 콜라겐 1, 콜라겐 4 유전자에 대한 유방암환자의 생존율을 분석, 예후인자로서의 의의를 확인하였다.

결과: miR-200b/200a/429 혹은 miR-141/200c 과발현은 MDA-MB-231 세포의 성장을 억제시켰고 이동, 침윤 능력을 증가시켰으며 세포 내 신호전달인자인 FAK 와 AKT 의 인산화를 증가시켰다. FAK 와 AKT 신호전달 억제제는 miR-200b/200a/429 혹은 miR-

141/200c 의 과발현에 의해 증가된 이동과 침윤능력을 억제하였다. 그리고 miR-200b/200a/429 과발현과 비교할 때, miR-141/200c 과발현은 MDA-MB-231 세포에서 VEGF-A 분비와 integrin-αV 발현을 현저하게 증가시켰다. VEGF-A 중화항체의 처리는 miR-200b/200a/429 혹은 miR-141/200c 과발현에 의해 증가된 MDA-MB-231 세포의 이동, 침윤 능력을 억제하였고 FAK 와 AKT 인산화를 감소시켰다. LOXL4 발현의 감소는 마우스 종양모델에서 MDA-MB-231 세포의 일차암 형성과 폐전이 능력을 증가시켰다. LOXL4 발현을 감소시킨 종양조직에서 PLOD1, PLOD2, P4HA1, P4HA2 뿐만아니라 콜라겐 1 과 콜라겐 4 의 발현이 현저하게 증가되었다. 또한 대조군에 비해 LOXL4 발현이 감소된 종양 조직 내 콜라겐 다발이 더 두꺼워지는 것을 관찰했다. 유방암 환자 (n=584)의 생존율 분석 결과, LOXL4 의 발현이 낮은 군에서는 생존율이 낮았으며 콜라겐 1 과 콜라겐 4 의 발현이 높고 LOXL4 발현이 낮은 군에서는 생존기간이 감소하였다. 특히 삼중음성 유방암 환자 (n=101)에서 LOXL4 발현이 낮고 콜라겐 1 과 콜라겐 4 의 발현이 높은 경우 생존율과 생존기간이 유의하게 감소하였다.

결론: 삼중음성 유방암세포에서 miR-141/200c 과발현은 VEGF-A 의 분비를 통해 세포 내 신호전달인자인 FAK 와 AKT 를 활성화 시켜 세포의 이동과 침윤능력을 촉진시켰다. 또한 LOXL4 의 발현억제는 종양조직의 콜라겐 합성을 증가, 축적 시키고 구조적 변화를 유도하여

일차암 성장과 폐전이를 증대시켰다. LOXL4 는 삼중음성 유방암 환자의 생존을 예측하는 예후인자로 역할을 할 수 있을 것으로 기대된다.

주요어: 삼중음성 유방암, 마이크로알엔에이-이백, 혈관내피성장인자, 라이실옥시데이즈-라이크 4 (LOXL4), 콜라겐, 암 진행, 전체 생존율

학번: 2012-31164